Supporting information for

"Insights into single-molecule magnet behavior from the experimental electron density of linear two-coordinate iron complexes"

Maja K. Thomsen[1], Andreas Nyvang[1], James P. S. Walsh[2], Philip C. Bunting[3], Jeffrey R. Long[3,4,5], Frank Neese*,[6] Michael Atanasov*[6,7], Alessandro Genoni,[8] Jacob Overgaard[1]*

[1] Department of Chemistry & Centre for Materials Crystallography, Aarhus University, DK-8000 Aarhus C, Denmark

[2] Department of Chemistry, Northwestern University, 2145 Sheridan Rd, Evanston, IL 60208 USA

[3] Department of Chemistry, University of California, Berkeley, California 94720-1460, USA

[4] Department of Chemical and Biomolecular Engineering, University of California, Berkeley, California 94720-1460, USA

[5] Materials Sciences Division, Lawrence Berkeley National Laboratory, Berkeley, California 94720, USA

[6] Department of Molecular Theory and Spectroscopy, Max Planck Institut für Kohlenforschung, Kaiser-Wilhelm Platz 1, D-45470 Mülheim an der Ruhr, Germany

[7] Institute of General and Inorganic Chemistry, Bulgarian Academy of Sciences, Sofia 1113, Bulgaria

[8] Université de Lorraine and CNRS, Laboratoire de Physique et Chimie Théoriques (LPCT), UMR CNRS 7019, 1 Boulevard Arago, F-57078 Metz, France.

Contents

1. Single crystal X-ray data collection and treatment 3

2. Experimental electron density modelling and analysis 5

3. *Ab initio* calculations 9

4. Theoretical structure factors 15

5. Theoretical electron density modeling and analysis 16

6. Evaluation of experimental multipole models 17

7. Doubling of the unit cell volume in 1 23

8. Local coordinate systems 24

9. Experimental multipole model parameters 36

10. Experimental electron density topology 44

11. Experimental atomic charges for iron 55

12. References 55

1. Single crystal X-ray data collection and treatment

The crystals of **1** and **2** are relatively air-sensitive and for that reason the selection and mounting had to happen within minutes to avoid crystal decomposition.

Single crystal X-ray diffraction data for **1** were collected using an Oxford Diffraction Supernova instrument at Aarhus University equipped with a Mo X-ray source, an Atlas charge-coupled device detector, and a four-circle goniometer. A selection of crystals were immersed in Fomblin oil and a suitable crystal was chosen, mounted on a nylon loop fixed to the goniometer head and placed in the Oxford Diffraction Supernova system, where the crystal was immediately cooled to 100(1) K using an Oxford Cryosystems liquid nitrogen Cryostream device. Initial screening of the crystal indicated that the limit of diffraction was at best 1.0 $Å^{-1}$. The data collection consisted of 26 omega scans, with a scan width of 1° per frame. The exposure time was set to 22.5 seconds at low angle (2θ = -1.25°) and 240 seconds at high angle (2θ = -133.102°/+130.602°). The unit cell parameters were determined and the Bragg intensities were integrated using CrysAlisPRO[1]. Frames affected by ice reflections and frames with an internal R-value above 7 % were subsequently omitted. The intensities were empirically corrected for absorption using SCALE3 ABSPACK implemented in CrysAlisPRO[1]. Outliers were rejected and equivalent reflections were averaged using SORTAV[2-3], giving 83820 unique reflections with a maximum resolution of $\sin(\theta)/\lambda$ = 0.98 $Å^{-1}$, an internal R-value of 4.83 %, a completeness of 98.9 %, and a redundancy of 5.6. The 2801 unique reflections, which had been measured only once, were hereafter omitted, giving the final number of 81019 accepted unique reflections corresponding to a completeness of 95.6 % and a redundancy of 5.8. The unit cell volume obtained for **1** was larger by a factor of ca. 2 compared to the cell previously reported in the literature[4]. Enforcing the previously published smaller cell while integrating the data, led to a large number of significant superstructure reflections at half-integer *k* values.

Single crystal X-ray diffraction data for **2** were measured at the beamline BL02B1 at the SPring-8 synchrotron in Japan. A suitable crystal was selected from Paratone-N oil, mounted on a thin glass fiber fixed to the goniometer head, and taken directly into a cold He gas-stream (ca 50 K) to preserve it. The diffractometer at BL02B1 is equipped with a large curved imaging plate detector with automatic readout mounted on a 3-circle goniometer, which has its chi-circle reduced to only one quarter of a full rotation. A relatively high X-ray energy (wavelength of 0.30988 Å) was chosen in order to reduce the risk of crystal decay by photodegradation, which we have previously observed for metal-organic complexes. The curved

imaging plate detector covers a large area, and data collection at the beamline is found to provide the best data using as wide omega scans as possible. For the present unit cell size a scan width of 6.5° per frame and an overlap of 0.5° between consecutive frames were chosen. A set of 24 frames was collected using an exposure time of 780 seconds per frame. The unit cell parameters were determined and the Bragg intensities were integrated using the software RAPID-AUTO[5]. An empirical absorption correction was applied. Outliers and symmetry forbidden reflections were rejected and equivalent reflections were averaged using SORTAV[2-3], giving 13457 unique reflections with a maximum resolution of $\sin(\theta)/\lambda = 1.02$ $Å^{-1}$, an internal R-value of 3.39 %, a completeness of 98.8 %, and a redundancy of 2.7.

Crystallographic details for **1** and **2** are listed in Table S1.

Table S1. Crystallographic details for **1** and **2**.

	1	**2**
Formula	$C_{38}H_{90}FeKN_2O_6Si_6$	$C_{20}H_{54}FeSi_6$
Formula weight [g/mol]	934.61	519.02
Crystal max, min dimension [μm]	288, 142	100, 30
Crystal system	Triclinic	Monoclinic
Space group	$P\bar{1}$	C2/c
T [K]	100(1)	50(1)
λ [Å]	0.71073	0.309880
a [Å]	12.80589(13)	16.0900(10)
b [Å]	15.65038(17)	8.8680(10)
c [Å]	27.4312(2)	23.0030(10)
α [°]	94.1171(7)	90
β [°]	97.3180(7)	111.317(1)
γ [°]	100.9749(9)	90
V [$Å^3$]	5327.06(9)	3057.7(4)
F(000)	2036	1136
ρ [g/cm^3]	1.165	1.127
Z	4	4
μ [mm^{-1}]	0.537	0.058

T_{min}, T_{max}	0.895,1.000	0.9440, 1.0884
$(\sin(\theta)/\lambda)_{max}$ [Å^{-1}]	0.9830	1.02
R_{int} [%]	4.83	3.39
N_{meas}	469046	36478
N_{unique}	81019 (≥2 contributors)	13457 (≥1 contributor)
Completeness [%]	95.6	98.8
Average redundancy	5.8	2.7

2. Experimental electron density modelling and analysis

The structures of compounds **1** and **2** were solved with direct methods using SHELXT[6] via the Olex2 interface[7], which located all non-hydrogen atoms. Hydrogen atoms were subsequently added in calculated positions, and the refinement was carried out by the least squares method using SHELXL-97[8] in Olex2[7]. A disorder model was tested for compound **1**, because some crypt-222 carbon and oxygen atoms have relatively elongated probability ellipsoids. In the disorder model, these atoms were split into two atoms. This did not diminish the residual electron density or the R-values, probably because of the disorder not being sufficiently pronounced. Thus each pair of ellipsoids corresponding to one of the split atoms overlap significantly, and they basically give rise to the same atomic electron density distribution of each disordered atom as does one elongated ellipsoid. For this reason, the disorder model was discarded.

The final multipole models of the electron density distributions in **1** and **2** were refined against the experimental $|F|^2 > 2\sigma(|F|^2)$ data in XD2006[9] using the atom-centered Hansen-Coppens formalism[10] with scattering factors from the SCM[11-13] data bank, and using statistical weights. Anomalous dispersion was taken into account and a harmonic thermal model was applied. Isotropic and anisotropic atomic displacement parameters (ADPs) were used for hydrogen and non-hydrogen atoms, respectively. Bond distances to the hydrogen atoms were fixed to values tabulated by Allen *et al*.[14] and the radial expansion/contraction parameters for hydrogen were fixed to values from Volkov *et al*.[15] (κ = 1.13 and κ' = 1.29).

For compound **1**, neutral atomic scattering factors were applied for all elements, except for potassium, for which an ionic (K^+) scattering factor was chosen. The default single-ζ slater type radial functions, with ζ values derived from Clementi and Raimondi[16], were used in the multipole scattering factors, $f_{lm\pm}$, for all non-iron atoms. For the iron atoms, the scattering contributions from the 4s shell and the 3d shell were

treated separately. Thus, the additional "4s" monopole population, P_{00}, referring to the f_{00} scattering factor, was refined. The corresponding radial expansion/contraction parameter, $\kappa'_{l=0}$, did not refine to a reasonable value and it was fixed to unity. For the f_{00} scattering factor, a 4s4s product radial function was applied. The 4s orbital is here expressed as an expansion of single-ζ slater type orbital (STO) basis functions with ζ_{STO} values and expansion coefficients from the SCM[11-13] data bank. For the $f_{2m\pm}$ and $f_{4m\pm}$ scattering factors, 3d3d product radial functions were applied. The 3d orbital is here expressed as an expansion of single-ζ slater type orbital (STO) basis functions with ζ_{STO} values and expansion coefficients from the SCM[11-13] data bank. The odd-order multipole populations are expected to be small based on the electronic configuration ($4s^1 3d^6$) of iron(I) and on the approximate local inversion symmetry on the iron atoms. For this reason default single-ζ slater type radial functions, with $\zeta = 2\cdot\zeta_{STO}(3d)$ obtained from Clementi and Raimondi[16], were chosen for the $f_{1m\pm}$ and $f_{3m\pm}$ scattering factors.

An initial refinement of non-hydrogen atomic positions and displacement parameters was carried out against the high-order data ($\sin(\theta)/\lambda > 0.8$ Å^{-1}). Thereafter, hydrogen atomic positions and displacement parameters were refined against the low-order data ($\sin(\theta)/\lambda < 0.7$ Å^{-1}). Finally, the high-order refinement of non-hydrogen atomic positions and displacement parameters was repeated.

Hydrogen atomic positions and displacement parameters were kept fixed at the obtained values during the following all-data refinements. More and more parameters were included while keeping a number of constraints in order to limit the number of parameters for the large asymmetric unit. Moreover, constraints were also applied in order to minimize the risk of modelling noise or disorder in the crypt-222 cryptands. Thus, only one common set of multipole populations was refined for each element in the $[K(crypt\text{-}222)]^+$ moieties. It was not possible to refine the monopole populations and the corresponding radial expansion/contraction parameter for the potassium atoms. This is to be expected, since a monovalent potassium ion formally has no valence electron density. These potassium parameters were therefore fixed to $\kappa = 1$ and $P_v = 0$, and the higher order multipole populations for potassium were fixed to zero (and κ' to unity) assuming a monovalent and spherical potassium ion. Furthermore, local approximate symmetries were used to reduce the number of multipole populations refined for nitrogen atoms in the $[K(crypt\text{-}222)]^+$ moieties.

For the $[Fe(C(SiMe_3)_3)_2]^-$ moieties, only one common set of multipole populations was refined for all methyl carbons, another common set of multipole populations was refined for all silicon atoms, and a third common set of multipole populations was refined for all hydrogen atoms. All the multipole populations of the C-Fe-C atoms were refined freely without constraints in order to maximize the model

flexibility in these regions. Local approximate symmetries were used to limit the number of multipole populations refined for hydrogen atoms in the $[Fe(C(SiMe_3)_3)_2]^-$ moieties. Thus, only one bond-directed dipole population (and the monopole population) was refined for these atoms. Finally, the sum of monopole population based charges of each $[K(crypt\text{-}222)]^+$ moiety was fixed to +1.

Multipole populations were refined to the level of dipoles and hexadecapoles for hydrogen atoms and non-hydrogen atoms, respectively, in the $[Fe(C(SiMe_3)_3)_2]^-$ moieties, whereas multipole populations to the level of monopoles and octupoles were refined for hydrogen atoms and non-hydrogen/non-potassium atoms, respectively, in the $[K(crypt\text{-}222)]^+$ moieties. One common set of radial expansion/contraction parameters (κ, κ') was refined for each of the elements: nitrogen, oxygen, silicon and iron, although the $\kappa'_{l=0}$ parameter for iron was fixed to unity (*vide supra*). Moreover, one common (κ, κ')-set was refined for each of the three groups of carbon atoms: iron-bonded carbon atoms, methyl carbon atoms in the $[Fe(C(SiMe_3)_3)_2]^-$ moieties, and crypt-222 carbon atoms. It was generally not possible to achieve convergence, when refining all radial expansion/contraction parameters simultaneously with all the other parameters. Some of the radial expansion/contraction parameters were therefore "block"-refined in limited parameter sets.

Finally, the crypt-222 hydrogen atomic displacement parameters (U_{iso}) were constrained to 1.5 times the value of the neighboring carbon, because some crypt-222 hydrogen U_{iso} values were unrealistically low. All parameters, except from the atomic positional and displacement parameters, were thereafter block-refined again. The very last refinement included only the multipole populations. The resulting final multipole model of the electron density in compound **1** is denoted **Model 3B**.

Compound **1** represents a challenging system for electron density modelling due to the very large asymmetric unit encompassing 288 atoms and due to the disorder in the $[K(crypt\text{-}222)]^+$ moieties. Thus, five electron density models (**Model 1A**, **Model 2A**, **Model 2B**, **Model 3A** and **Model 3B**), differing in the choice of scattering factors and in the level of model sophistication for the crypt-222 atoms, were compared, before choosing the final model (**Model 3B**) described above. In order to justify the rather elaborate multipole model for the slightly disordered $[K(crypt\text{-}222)]^+$ moieties, three levels of increasing sophistication were compared for the crypt-222 atoms: an independent atom model (**Model 1A**), a kappa model[17] (**Model 2A** and **Model 2B**), and a multipole model[10] (**Model 3A** and **Model 3B**). In all cases, a multipole model was applied simultaneously for the $[Fe(C(SiMe_3)_3)_2]^-$ atoms. **A** refers to the choice of neutral scattering factors for all elements from the VM data bank in XD2006[9]. **B** refers to the choice of ionic (K^+) scattering factors for potassium and neutral scattering factors for all other elements from the

SCM[11-13] data bank in XD2006[9]. When the level of model sophistication for the crypt-222 atoms is increased from the independent atom model (**Model 1A**) to the kappa model (**Model 2A and Model 2B**) and finally to the multipole model (**Model 3A and Model 3B**), the R-values and the residual electron density peaks/troughs decrease and the goodness-of-fit becomes closer to unity. Furthermore, the **B**-scattering factors perform better than the **A**-scattering factors with respect to these measures. Likewise, a residual-density analysis[18] reveals a decrease in the number of gross residual electrons in the unit cell and a more narrow fractal dimension distribution, as the level of model sophistication is increased for the crypt-222 atoms and when choosing the **B**-scattering factors instead of the **A**-scattering factors. When evaluating binned $\Sigma F_o^2/\Sigma F_c^2$-values as a function of $\sin(\theta)/\lambda$, all five models exhibit severe discrepancies between the experimental and calculated data at low $\sin(\theta)/\lambda$-values, though most pronounced when using the independent atom model for the crypt-222 atoms and/or using **A**-scattering factors. Moreover, the normal probability plots become slightly more satisfying when increasing the model sophistication for the crypt-222 atoms and when applying the **B**-scattering factors rather than the **A**-scattering factors. According to the above remarks, **Model 3B** was chosen as the final electron density model for compound **1**.

For compound **2**, neutral atomic scattering factors were applied for all elements, except for iron, for which an ionic (Fe^{2+}) scattering factor was chosen. The default single-ζ slater type radial functions, with ζ values derived from Clementi and Raimondi[16], were used in the multipole scattering factors, $f_{lm\pm}$, for all atoms. Initially, the non-hydrogen and hydrogen atomic positions and displacement parameters were refined from high-order and low-order data, respectively, in the exact same way as done for compound **1**. Hydrogen atomic positions and displacement parameters were kept fixed at the obtained values during the following all-data refinements. More and more parameters were included while releasing all constraints for the multipole populations, except for the constraints on the hydrogen atoms, for which only one common monopole population and one common bond-directed dipole population were refined. Multipole populations were refined to the level of dipoles and hexadecapoles for hydrogen atoms and non-hydrogen atoms, respectively.

Both radial expansion/contraction parameters (κ and κ') were refined for iron. Moreover, one common κ parameter was refined for all methyl carbon atoms, and another κ parameter was refined for the iron-bonded carbon atom. The κ parameter refined to an unphysical value for silicon, and it was therefore fixed to unity for the silicon atoms. The κ' parameter refined to unphysical values for both carbon and silicon atoms, and it was therefore fixed to unity for these atoms.

A topological analysis[19] of the multipole model electron density in **1** and **2** was carried out with the XDPROP module in XD2006[9]. This module was also used to calculate experimental d-orbital occupancy estimates for the iron atoms in **1** and **2** from the multipole populations according to the procedure from Holladay *et al*.[20]

3. *Ab initio* calculations

Input data for the ORCA calculations on the $Fe^{I}C_2$ and $Fe^{II}C_2$ complexes are listed below.

Input for FeIC2 Fe site 1

```
! DKH DKH-DEF2-TZVP AUTOAUX NoFrozenCore TIGHTSCF PAL8 KeepDens
PrintBasis PrintMos

%scf
maxcore 8000
end

%rel
picturechange 2
end

%casscf
nel 7
norb 5
mult 4
nroots 10
actorbs dorbs
printwf true
trafostep rimo
switchstep nr
nevpt2 true
nevpt
D4Tpre 1e-13
end
rel
dosoc true
gtensor true
printlevel 3
end
end

*xyz  -1  4
Fe     -0.513159   13.099877   22.504480
Si     -2.450717   11.470330   20.661425
Si     -3.295958   14.304565   21.555227
Si     -3.191379   12.002071   23.629260
Si      2.405291   11.902470   22.541085
```

Si	1.553346	13.886328	24.749491
Si	1.915711	14.903246	21.843821
C	-2.489892	12.704960	22.055087
C	-2.091335	9.702950	21.211970
C	-4.088005	11.325702	19.714718
C	-1.146272	11.797058	19.335125
C	-2.942560	14.827167	19.770763
C	-2.786290	15.820752	22.557872
C	-5.190607	14.244031	21.628384
C	-4.784849	11.002159	23.400448
C	-3.669878	13.312759	24.902573
C	-2.034498	10.852885	24.580921
C	1.468223	13.465411	22.939359
C	2.748535	11.641735	20.708373
C	4.137532	11.828034	23.310017
C	1.557744	10.298797	23.071757
C	1.506792	12.405878	25.914098
C	0.184911	15.013043	25.396152
C	3.165594	14.764250	25.243178
C	3.784887	15.125327	21.592645
C	1.348905	16.580419	22.504534
C	1.220351	14.830822	20.093498
H	-1.135350	9.644898	21.679827
H	-2.049053	9.085646	20.343672
H	-2.810894	9.334178	21.906716
H	-4.887395	11.074321	20.373725
H	-4.001713	10.556241	18.981795
H	-4.373488	12.237915	19.243070
H	-1.164094	12.787327	18.940912
H	-1.271347	11.093594	18.543991
H	-0.160964	11.670824	19.722028
H	-1.908854	15.030992	19.608583
H	-3.458426	15.735113	19.556058
H	-3.289162	14.167719	19.008329
H	-2.880940	15.740221	23.616778
H	-3.400868	16.639675	22.261670
H	-1.767768	16.041324	22.333690
H	-5.558555	13.485804	20.975875
H	-5.568375	15.181857	21.290487
H	-5.567181	14.058997	22.608502
H	-5.563525	11.608415	22.997571
H	-5.134257	10.766812	24.379754
H	-4.664710	10.092663	22.857322
H	-2.838520	13.923595	25.171158
H	-4.071939	12.841875	25.770330
H	-4.435453	13.965494	24.550056
H	-1.618091	10.040626	24.030214
H	-2.506112	10.464249	25.454363
H	-1.180703	11.395943	24.916382
H	1.866151	11.659535	20.110285
H	3.280445	10.730271	20.558648
H	3.316824	12.450702	20.309557

```
H       4.736429   12.657674   23.011108
H       4.623817   10.941937   22.971037
H       4.109278   11.844575   24.375422
H       1.232243   10.307731   24.086801
H       2.232226    9.491794   22.897393
H       0.706841   10.136198   22.450654
H       0.619706   11.820332   25.833685
H       1.532761   12.814421   26.898277
H       2.344694   11.756377   25.803090
H       0.055387   15.899517   24.818370
H       0.407865   15.333539   26.388183
H      -0.741541   14.489853   25.461674
H       4.001856   14.143136   25.016289
H       3.203468   14.978243   26.286651
H       3.305418   15.704931   24.761783
H       4.294953   15.245047   22.520779
H       3.944035   16.003706   21.009719
H       4.231319   14.314067   21.064410
H       0.291253   16.653891   22.615812
H       1.623260   17.294130   21.761594
H       1.752127   16.867100   23.448642
H       1.371881   13.887848   19.619955
H       1.676126   15.604381   19.518694
H       0.174332   15.032229   20.130862
*
```

Input for $Fe^{II}C_2$

```
! DKH DKH-DEF2-TZVP AUTOAUX NoFrozenCore TIGHTSCF PAL8 KeepDens
printbasis printmos

%scf
maxcore 8000
end

%rel
picturechange 2
end

%casscf
nel 6
norb 5
mult 5
nroots 5
actorbs dorbs
printwf true
trafostep rimo
switchstep nr
nevpt2 true
```

```
nevpt
D4Tpre 1e-13
end
rel
dosoc true
gtensor true
printlevel 3
end
end

*xyz  0  5
Fe      0.000000    0.000000    0.000000
Si     -0.662853   -1.821922    2.527126
Si      2.231584   -0.773210    2.013682
Si      0.031056    1.189358    2.985068
C       0.394367   -0.361371    1.982459
C       3.030460   -0.556733    3.701682
C      -0.131487    0.852481    4.829652
C       1.310772    2.563295    2.820513
C      -0.002989   -2.698178    4.060407
C       2.634435   -2.532612    1.476901
C      -0.805079   -3.096262    1.147749
C      -2.451634   -1.404957    2.951017
C      -1.583062    1.990423    2.448716
C       3.167962    0.318095    0.793309
H       2.991713    0.441688    4.073029
H       4.051235   -0.856959    3.636387
H       2.542404   -1.191017    4.405846
H      -0.895772    0.124391    4.978692
H      -0.389900    1.734794    5.369282
H       0.782457    0.483581    5.235585
H       2.292965    2.278349    3.121358
H       1.019862    3.344948    3.484283
H       1.421334    2.941214    1.829841
H       0.984532   -3.066608    3.901381
H      -0.665163   -3.507941    4.265721
H      -0.006755   -2.092529    4.937634
H       2.275161   -3.272496    2.155136
H       3.698791   -2.573964    1.433807
H       2.274742   -2.767862    0.501465
H      -1.293483   -2.662227    0.305431
H      -1.397554   -3.909059    1.500516
H       0.134528   -3.430293    0.770680
H      -2.510535   -0.703702    3.751741
H      -2.859772   -2.346836    3.238447
H      -3.019368   -0.997535    2.146029
H      -1.494467    2.270802    1.424121
H      -1.734202    2.863796    3.041041
H      -2.413148    1.328905    2.546776
H       2.849857    0.082898   -0.196506
H       4.197739    0.052711    0.867155
H       3.062594    1.359012    0.997851
```

Si	0.662853	1.821922	-2.527126
Si	-2.231584	0.773210	-2.013682
Si	-0.031056	-1.189358	-2.985068
C	-0.394367	0.361371	-1.982459
C	-3.030460	0.556733	-3.701682
C	0.131487	-0.852481	-4.829652
C	-1.310772	-2.563295	-2.820513
C	0.002989	2.698178	-4.060407
C	-2.634435	2.532612	-1.476901
C	0.805079	3.096262	-1.147749
C	2.451634	1.404957	-2.951017
C	1.583062	-1.990423	-2.448716
C	-3.167962	-0.318095	-0.793309
H	-2.991713	-0.441688	-4.073029
H	-4.051235	0.856959	-3.636387
H	-2.542404	1.191017	-4.405846
H	0.895772	-0.124391	-4.978692
H	0.389900	-1.734794	-5.369282
H	-0.782457	-0.483581	-5.235585
H	-2.292965	-2.278349	-3.121358
H	-1.019862	-3.344948	-3.484283
H	-1.421334	-2.941214	-1.829841
H	-0.984532	3.066608	-3.901381
H	0.665163	3.507941	-4.265721
H	0.006755	2.092529	-4.937634
H	-2.275161	3.272496	-2.155136
H	-3.698791	2.573964	-1.433807
H	-2.274742	2.767862	-0.501465
H	1.293483	2.662227	-0.305431
H	1.397554	3.909059	-1.500516
H	-0.134528	3.430293	-0.770680
H	2.510535	0.703702	-3.751741
H	2.859772	2.346836	-3.238447
H	3.019368	0.997535	-2.146029
H	1.494467	-2.270802	-1.424121
H	1.734202	-2.863796	-3.041041
H	2.413148	-1.328905	-2.546776
H	-2.849857	-0.082898	0.196506
H	-4.197739	-0.052711	-0.867155
H	-3.062594	-1.359012	-0.997851

*

Discussion of the results in relation with the data based on the structures reported previously.

Calculations yield ab initio ligand field orbital energies and magnetic sublevels split out by spin-orbit coupling from the ^4E and ^5E ground states of $Fe^{I}C_2$ and $Fe^{II}C_2$. Geometrical parameters resulting from the two different X-ray structural determinations of $Fe^{I}C_2$ (the one of this work in comparison with the structure previously reported[4]) and $Fe^{II}C_2$ (reported here and previously[21]) are listed in Table S2.

Differences between energies computed using the old and the new structures are very small, showing that the lowest electronic sublevels responsible for the magnetic behavior remain essentially unchanged.

Table S2. Geometrical parameters, NEVPT2 ab-initio ligand field 3d-MO energies and spin-orbit magnetic sublevels for $Fe^{I}C_2$ and $Fe^{II}C_2$ computed using the new structures (reported in this work) and the ones published previously.

Parameters	$Fe^{I}C_2$		$Fe^{II}C_2$	
	$Fe(1)C_2$, this work	Ref.4	FeC_2,this work	Ref.22
R(Fe-C)/Å	2.061,2.065	2.058,2.062	2.053	2.045
∠CFeC/°	179.1	179.2	180.0	180.0
∠SiC(Fe)CSi/°	30.1,30.3,30.9	21.8,22.1,22.2	57.8,61.0,61.3	58.7,60.5,60.8
AILFT MO energies/cm^{-1}				
$d_{x2-y2,xy}$	4717,4807	4696,4763	0,100	0,91
$d_{xz,yz}$	6970,7028	7008,7066	4406,4157	4503,4454
d_{z2}	0	0	3841	3560
$^4E/^5E$ D_3'/D_3 SOC sublevels/cm^{-1}				
Γ_4 / E(1)	0	0	0,0	0,0
Γ_4/ A_1,A_2(1)	217	218	188,189	190,190
Γ_{56}/ E(2)	464	460	341,440	346,437
Γ_{56}/ E(3)	712	710	596,600	596,598
- /A_1,A_2(1)	-		801,801	801,801

Effect of Spin-Orbit Coupling on the 3d-orbital populations in the $Fe^{I}C_2^{1-}$ SMM

CASSCF calculations on the $Fe^{I}C_2^{1-}$ single ion magnet were done using the already reported X-ray geometry,[4] which was reoriented such that one z-axis coincides with one of the two Fe-C bonds. This geometry deviates only slightly from the geometries of the Fe(1) and Fe(2) complexes of the X-ray structure reported here. The complex deviates slightly from the C-Fe-C geometry: with Fe at (0,0,0) the

coordinates of the two carbon ligands are 0, 0, 2.063 and -0.013, 0.026, -2.057. Orbital energies from ab-initio ligand field (AILFT) CASSCF calculations (in cm^{-1}) are 0.0 (d_{z2}), 3138, 3180 (d_{xy},d_{x2-y2}) and 4728, 4739 (d_{xz},d_{yz}). The splittings of d_{xy},d_{x2-y2} (42 cm^{-1}) and d_{xz},d_{yz} (11 cm^{-1}) reflects the minor deviations from the trigonal symmetry; after averaging one gets 0, 3159 and 4734 cm^{-1} for orbital energies of (d_{z2}), (d_{xy},d_{x2-y2}) and (d_{xz},d_{yz}) representative for the higher D_3 complex pseudosymmetry. Introducing these energies along with the Racah B=947 cm^{-1} and spin-orbit coupling ς=347 cm^{-1} parameters from the AILFT/CASSCF calculations into the ligand field program AOMX, we get the following 3d orbital populations in the ^4E ground state of the complex (ς=0, symmetry notations pertain to the D_3 idealised point group of the complex): $d_{xy}^{1.5}$ d_{xz}^{1} d_{yz}^{1} $d_{x2-y2}^{1.5}$, d_{z2}^{2}. Accounting for spin-orbit coupling (ς=347 cm^{-1}) the ^4E state splits into four Kramers doublets with symmetries (with Bethe notations for the irreducible representations of the D_3' double group), energies and 3d orbital populations listed in Table S3. From these model calculations we can conclude that the spin-orbit coupling does not essentially modify the 3d-orbital populations of the spin-orbit split sublevels of ^4E ground state of the complex. This is also expected given that non-relativistic and relativistic eigenfuctions share basically the same spatial part, small deviation being due to spin-orbit mixing of excited state multiplets into the ground state wave function. Since metal-ligand covalence in the considered complexes, both in $Fe^{I}C_2^{1-}$ and $Fe^{II}C_2$ is very weak we can considered these results to a very good approximation as rigorous.

Table S3. Symmetries, energies and 3d-orbital populations of the four spin-orbit Kramers doublet sublevels split out from the ^4E non-relativistic ground state of the $Fe^{I}C_2^{1-}$ single ion magnet.

Symmetry (D_3')	Energy (cm^{-1})	n_{dxy}	n_{dxz}	n_{dyz}	n_{dx2-y2}	n_{dz2}
Γ_4	0	1.500	1.002	1.002	1.500	1.997
Γ_4	195	1.498	1.006	1.006	1.498	1.992
Γ_{56}	420	1.497	1.008	1.008	1.497	1.991
Γ_{56}	673	1.497	1.005	1.005	1.497	1.994

4. Theoretical structure factors

As described in the previous section, ORCA was used to calculate the electronic structure of both mono- and di-valent Fe-complexes. In order to obtain theoretical d-orbital occupancies comparable to the experimentally derived ones, we calculated theoretical structure factors exploiting the density matrices obtained from the CASSCF calculations performed through ORCA. In particular, this has been done by exploiting a routine of the XC-ELMO program[22] that computes the structure factors as the trace of the matrix product between the one-electron density matrix and the matrix of the Fourier transform integrals of the basis function products, with the latter evaluated by extending the Obara-Saika and Head-Gordon-Pople recurrence relations for molecular integrals[23-24]. The calculations of the theoretical structure factors have been carried out by placing a single molecule inside a cubic cell with side lengths of 20 Å and constructing an infinite crystal from this. We calculated all possible 658212 structure factors to a resolution of 1.7 $Å^{-1}$ and used XD[25] to perform a multipole refinement against F with phases restricted to the calculated ones.

5. Theoretical electron density modeling and analysis

In the following the refinement of one (Fe1) of the Fe-complexes in **1** is described. The atomic coordinates are fixed to the ones used for the calculation, which also correspond to the final experimental coordinates. The final model consists of multipoles up to hexadecapoles for Fe and Si, while up to octupoles are used for carbon, and a bond-directed dipole and quadrupole common to all hydrogen atom. Five different radial scaling parameters are used for the spherical valence functions, one for each atom type, except for carbon where we separate the methyl-C from the two C-atoms directly bonded to Fe. The radial scaling parameters for the deformation functions (κ'') are refined in separate cycles for convergence purposes. At this stage, significant residuals density maxima were found with 0.04 Å of the atomic positions. These are well-known effects of the effect of chemical bonding on the core electron density,[26-28] and can be removed by radial scaling of the different shells of electron density. The way that XD is constructed allows for the use of a so-called extended Hansen-Coppens model in which we refine radial scaling parameters for three shells on Fe (K, L, and M), two shells on Si (K and L), and the 1s electron on carbon atoms. This reduces the residual significantly, and the final model exhibits maximum and minimum residuals of $\pm$0.25 $eÅ^{-3}$ for the full data set.

A completely analogous procedure was used for compound **2**. A selected list of crystallographic details and refinement results are given in Table S4.

Table S4. Refinement statistics and results for the final multipole models using theoretical structure factors calculated for compounds **1** and **2**.		
	1’	2’
Crystal system	Triclinic	
Space group	P1	
a, b, c [Å]	20	
α, β, γ [°]	90	
Z	1	
$(\sin(\theta)/\lambda)_{max}$ [$Å^{-1}$]	1.7	
N_{obs}	658202	658212
N_{par}	504	259
R(F) [%]	0.13	0.21
$\Delta\rho_{max}$ [$eÅ^{-3}$]	0.25	0.33
$\Delta\rho_{min}$ [$eÅ^{-3}$]	-0.24	-0.32
$\Delta\rho_{rms}$ [$eÅ^{-3}$]	0.003	0.007
κ(Fe-K)	0.9271(5)	1.00176(2)
κ(Fe-L)	1.01408(4)	1.00076(2)
κ(Fe-M)	1.01033(3)	1.0300(5)
κ(Si-K)	1.00373(1)	0.99447(2)
κ(Si-L)	1.01117(3)	1.00266(1)
κ(C-K)	0.99080(2),0.99521(1)	0.98952(2),0.99733(1)

6. Evaluation of experimental multipole models

Results from the multipole model refinements of compounds **1** and **2** are listed in Table S5.

Table S5. Refinement statistics and results for the final multipole models of compounds **1** and **2**. N_{par} is the number of parameters refined simultaneously in the last refinement.		
	1	**2**
Weighting scheme	$1/\sigma^2(F_o^2)$	$1/\sigma^2(F_o^2)$

N_{obs} ($F_o^2 > 2\sigma(F_o^2)$)	57034	10223
N_{par}	242	470
$R(F^2)$ [%]	3.88	2.95
$R_{all}(F^2)$ [%]	4.48	3.44
$R_w(F^2)$ [%]	6.25	4.04
GoF	1.1706	0.8715
$\Delta\rho_{max}$ [eÅ^{-3}]	0.882[i]	0.55[ii]
$\Delta\rho_{min}$ [eÅ^{-3}]	-0.431	-0.32
$\Delta\rho_{rms}$ [eÅ^{-3}]	0.075	0.062

[i] Maximum residual electron density peaks are positioned ca. 0.1 Å from the potassium centers.

[ii] Maximum residual electron density peak is positioned 0.01 Å from the iron center.

Selected residual electron density maps are depicted in Fig. S1 for **1** and **2**. The highest peaks in **1** are positioned near the potassium atoms (0.88 eÅ^{-3} 0.10 Å from K1 and 0.72 eÅ^{-3} 0.12 Å from K1A) and near the iron atoms (0.54 eÅ^{-3} 0.17 Å from Fe1 and 0.56 eÅ^{-3} 0.17 Å from Fe2). The highest silicon peaks amount to 0.51 eÅ^{-3}. Moreover, there are some significant residual electron density features in the crypt-222 regions with peaks typically positioned 0.4-0.9 Å from the non-hydrogen atom centers. These features are most likely a result of disordered crypt-222 atoms. The highest peak in these regions amounts to 0.48 eÅ^{-3}. There are no more peaks/troughs with absolute values greater than 0.40 eÅ^{-3} in **1**. In **2**, the highest peak of 0.55 eÅ^{-3} resides only 0.01 Å from the iron center. Likewise, the second-highest peak of 0.43 eÅ^{-3} is positioned only 0.05 Å from silicon in **2**. The highest peak might be a result of iron being located on a special position (with $\bar{1}$ site symmetry), since errors tend to accumulate near special positions in the unit cell.[29-30] The iron and silicon core residual electron density might indicate a problem with the scale factor or a need for improved radial functions for these atoms. Indeed, the radial expansion/contraction parameters (κ and κ') were not refined for silicon, because the refinement led to unphysical values.

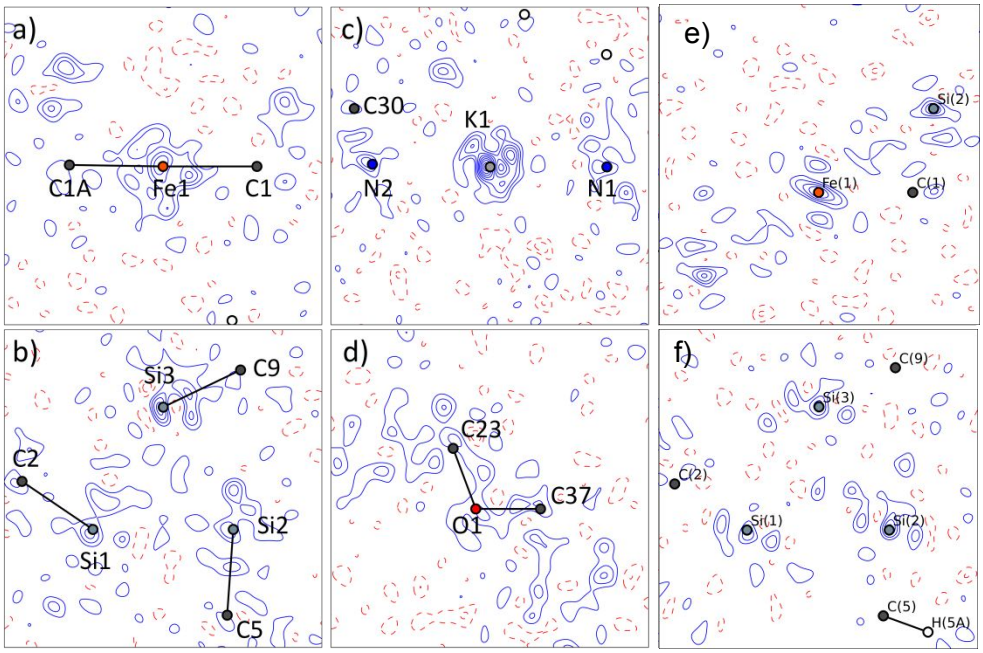

Figure S1. Selected residual electron density maps from the multipole models of **1** (a, b, c, d) and **2** (e, f). Contours are drawn with increments of 0.1 eÅ^{-3}. Positive and negative contours are plotted with solid blue and dashed red lines, respectively. These plots have been created using a modified version of QuickPlot[31].

The static model deformation electron density has been evaluated in **1** and **2**. Fig. S2 shows selected planes from the crypt-222 regions in **1**. Fig. S3 shows selected planes containing Si-C bonds from the $C(SiMe_3)_3$ ligands in **1** and **2**. The maps in Fig. S2 and Fig. S3 exhibit the expected bonding features, indicating that the multipole model parameters fit chemical bonding features and not simply noise and/or disorder.

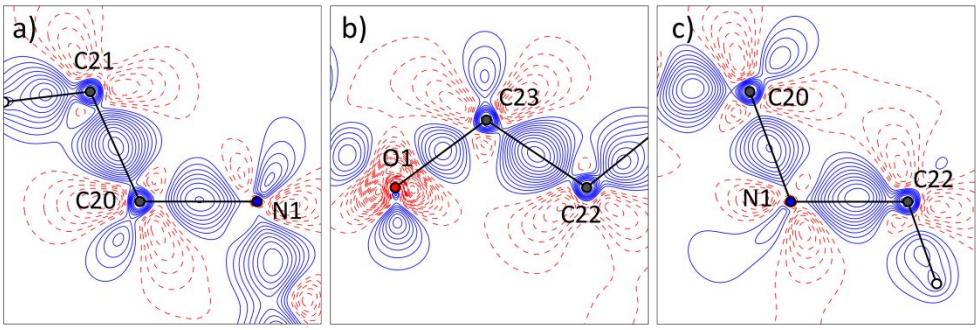

Figure S2. Selected static model deformation electron density maps in the crypt-222 regions of **1**. Contours are drawn with increments of 0.05 eÅ^{-3}. Positive and negative contours are plotted with solid blue and dashed red lines, respectively. These plots have been created using a modified version of QuickPlot[31].

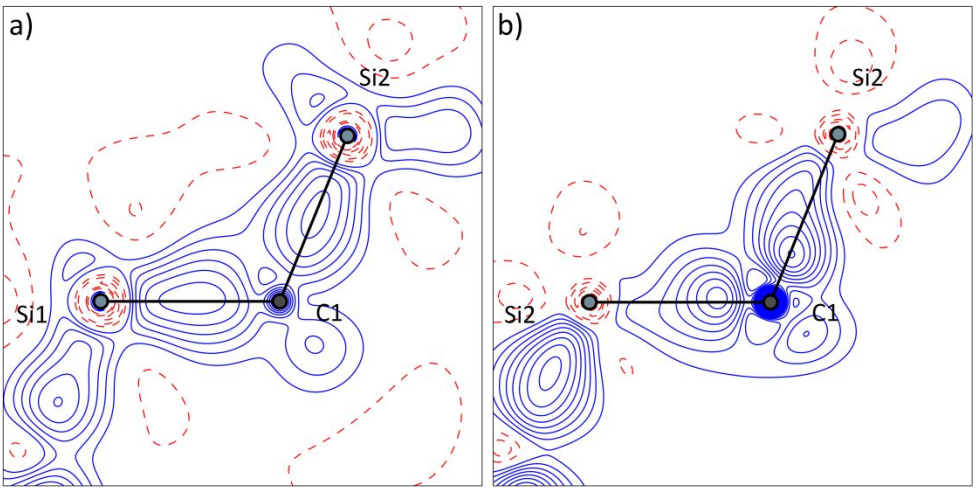

Figure S3. Selected static model deformation electron density maps in one of the $[Fe(C(SiMe_3)_3)_2]^-$ ions in **1** (a) and in the $Fe(C(SiMe_3)_3)_2$ molecule in **2** (b). Contours are drawn with increments of 0.05 eÅ^{-3}. Positive and negative contours are plotted with solid blue and dashed red lines, respectively. These plots have been created using a modified version of QuickPlot[31].

Hirshfeld's rigid-bond test[32] has been applied to the non-hydrogen and non-metal atom pairs in compounds **1** and **2**. The largest differences in mean square displacement amplitudes for covalently bonded pairs in **1** are generally found for crypt-222 atoms with the maximum value of 0.022 Å^2.This is to be expected due to the un-modelled disorder in these moieties, which has instead been absorbed to some extent in the atomic displacement parameters. The maximum difference in mean square displacement amplitudes for the Si-C bonds is 0.018 Å^2 in **1** and 0.019 Å^2 **2**.This is considered acceptable owing to the mass difference between carbon and silicon.

The scale factor as a function of resolution, ($\sin(\theta)/\lambda$, $\Sigma F_o^2/\Sigma F_c^2$), is plotted in Fig. S4 for compounds **1** and **2**. These plots should ideally exhibit values near unity across the entire resolution range, corresponding to a constant scale factor[33]. The plots in Fig. S4, however, exhibit substantial discrepancies between

experimental and calculated data at low-order for both compounds **1** and **2**. Moreover, the plot for compound **2** shows disagreement at high-order.

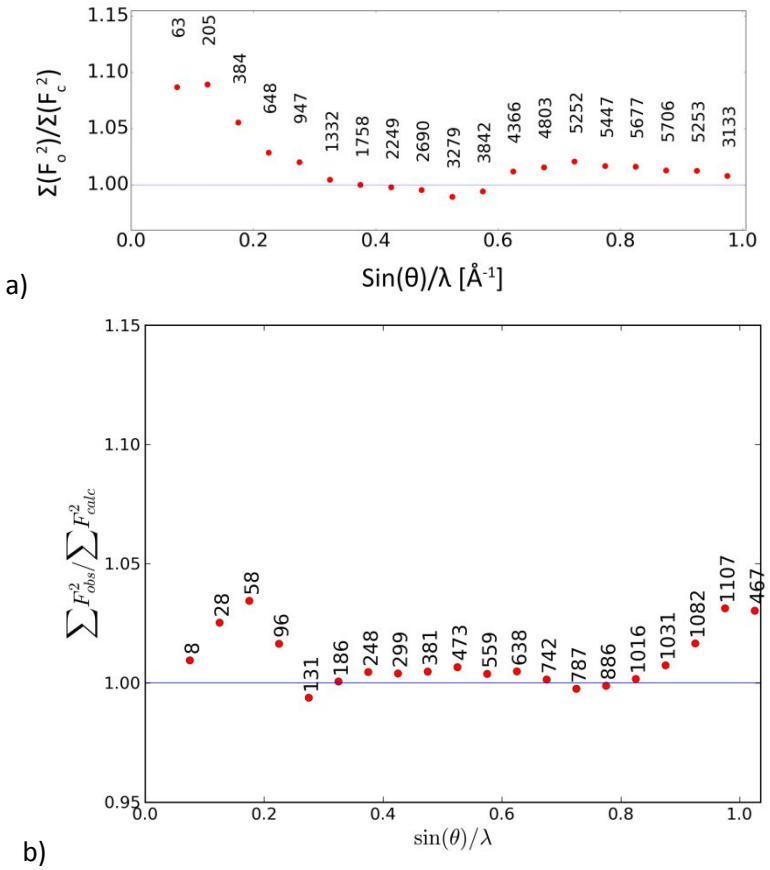

Figure S4. $\Sigma F_o^2/\Sigma F_c^2$ plotted against sin(θ)/λ for the final multipole models of compound **1** (a) and **2** (b). The numbers of reflections included in the bins are included in the figure (vertical numbers). These plots have been obtained using a modified version of fco_plot.[34]

Normal probability plots[35] are provided in Fig. S5 for compounds **1** and **2**. These should be straight lines with unity slope and zero intercept in the case of correctly assigned standard uncertainties and no systematic errors. These plots are reasonable for both compounds **1** and **2**.

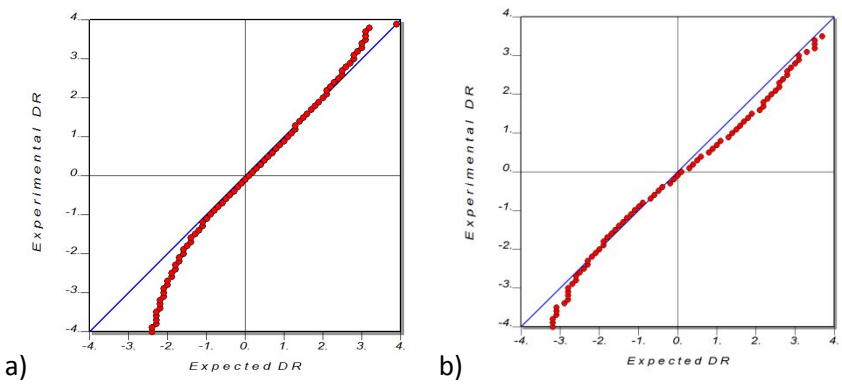

Figure S5. Normal probability plots based on F^2 for the final multipole models of compound **1** (a) and **2** (b). These plots have been obtained using the DRK-Plot[36] utility in WinXD v1.04[25].

The residual-density analysis developed by Meindl and Henn[18] has been applied to evaluate descriptors of the residual electron density in compounds **1** and **2**. The results are provided in Fig. S6. It appears that the fractal dimension distribution plotted against the residual electron density, $d^f(\Delta\rho)$, becomes much more parabolic when only a part of the unit cell corresponding to one $[Fe(C(SiMe_3)_3)_2]^-$ moiety in compound **1** is included (Fig. S6 (c)).

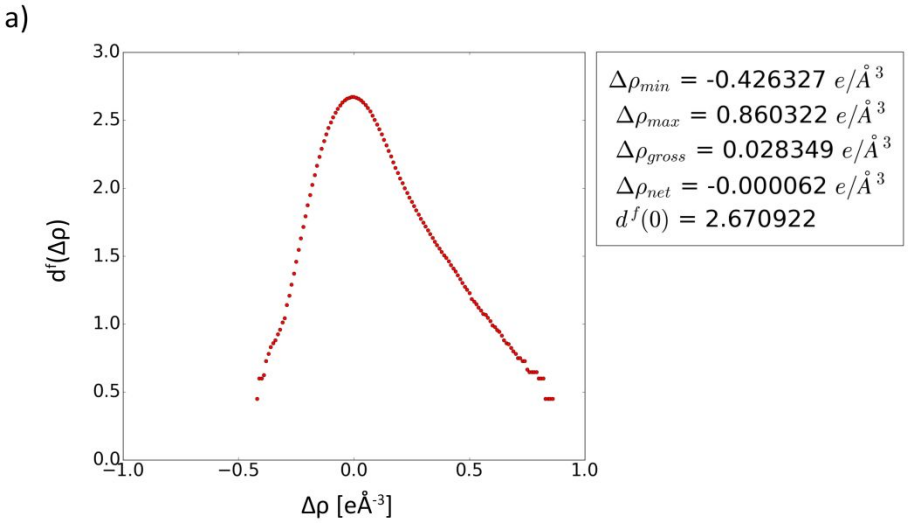

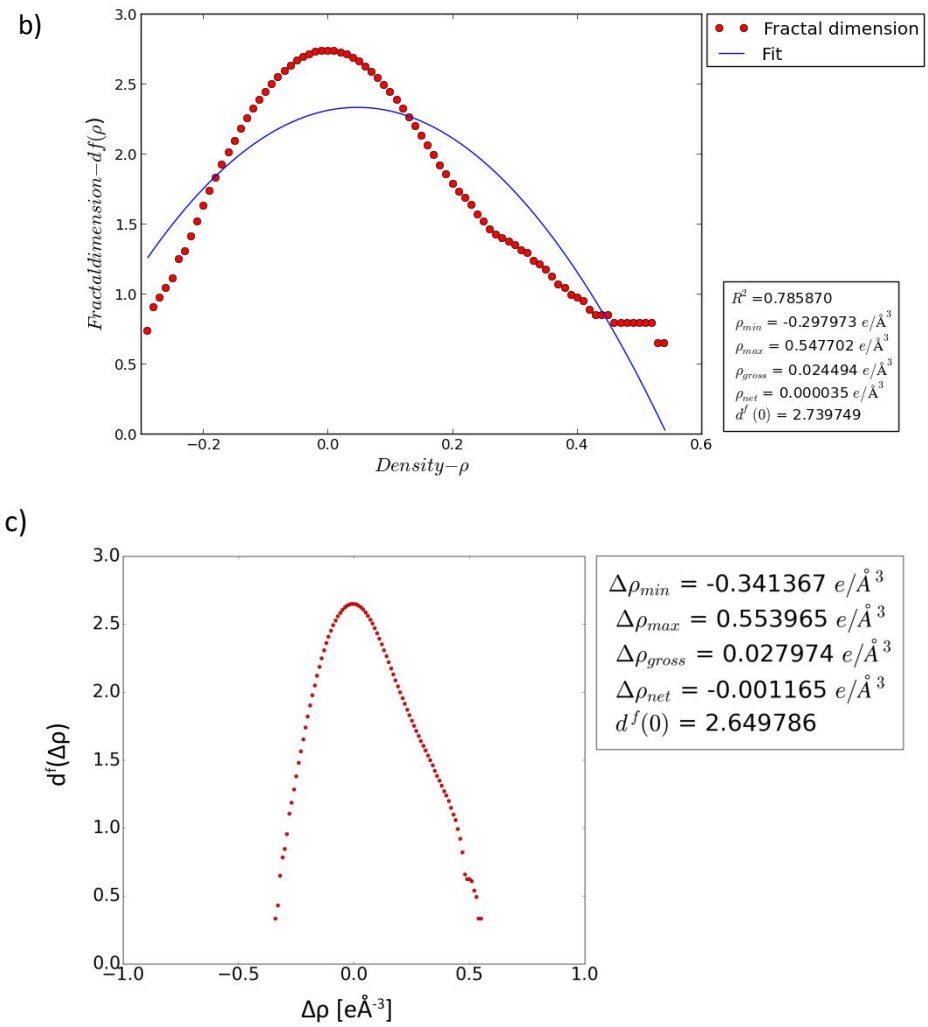

Figure S6. Fractal dimension distribution (d^f) plotted against the residual electron density (red dots) for the final multipole models of compound **1** (a) and **2** (b) and including the whole unit cell. The same plot including only a part of the unit cell corresponding to one $[Fe(C(SiMe_3)_3)_2]^-$ moiety in compound **1** is also provided (c).These plots have been obtained using the local program RDA.

7. Doubling of the unit cell volume in 1

The unit cell parameters found for **1** did not match the ones previously reported[4]. Instead, a unit cell having a volume twice as large appeared. The new structure of **1** features two geometrically distinct $[Fe(C(SiMe_3)_3)_2]^-$ moieties (in contrast to the previously published[4] structure, which contains only one $[Fe(C(SiMe_3)_3)_2]^-$ moiety in the asymmetric unit). The structural differences between the two $[Fe(C(SiMe_3)_3)_2]^-$ moieties are mainly found in the relative orientation of the two $C(SiMe_3)_3$-ligands around

the C-Fe-C line, quantified by the Si-C-C-Si torsion angle. These torsion angles vary between 14.4-14.8° in one of the $[Fe(C(SiMe_3)_3)_2]^-$ moieties and between 30.1-30.9° in other. The corresponding torsion angles from the previously reported structure[4] are very close to the average of these values (21.8-22.2°). The ellipsoids of the $C(SiMe_3)_3$-ligands from the previously published model[4] are elongated in the directions corresponding to a rotation of one of the $C(SiMe_3)_3$-ligands with respect to the other one around the C-Fe-C line. This is much less pronounced for the multipole model of **1** obtained in the present study, where the ellipsoids are smaller and more isotropic, although the data collection temperature was 100 K in both experiments. Fig. S7 (a) shows the atomic probability ellipsoids in one of the $[Fe(C(SiMe_3)_3)_2]^-$ moieties from the multipole model of **1** obtained in the present study. Fig. S7 (b) shows the ellipsoids from the previously reported model[4] of **1**. These elongated ellipsoids seem to be a result of an average molecular geometry of the two correct geometries.

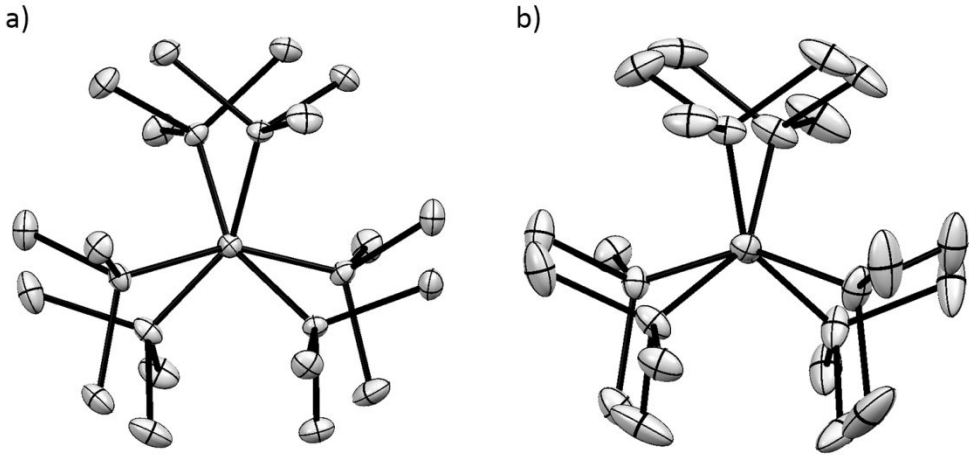

Figure S7. 50 % probability ellipsoids for one of the $[Fe(C(SiMe_3)_3)_2]^-$ moieties from the multipole model of **1** obtained in the present study (a) and for the single $[Fe(C(SiMe_3)_3)_2]^-$ moiety previously reported[4] (b). The Fe-C bonds are roughly orthogonal to the paper plane and hydrogen atoms are omitted for clarity. This figure has been created using Mercury 3.5.1[37].

8. Local coordinate systems

The local coordinate systems used in the experimental multipole modelling of compounds **1** and **2** are provided in Table S6 and Table S7. **ax1**, **ax2**, and **ax3** refer to different local axis assignments, each being

either **x**, **y**, or **z**. **v1** is the vector from atom to atom0. **v2** is the vector from atom1 to atom2. The vector **v3** is given by the cross product **v1** × **v2** . The unit axes of the local coordinate system are then given as: e_{ax1} = **v1**/|**v1**|, e_{ax2} = **v3** × **v1**/|**v3** × **v1**|, and e_{ax3} = **v3**/|**v3**|.

Table S6. Local atomic right-handed coordinate systems applied in the multipole modelling of compound **1**.

atom	atom0	ax1	atom1	atom2	ax2
Fe1	C1A	Z	Fe1	C1	Y
Fe2	C1B	Z	Fe2	C1C	Y
K1	N1	Z	K1	O5	Y
K1A	N1A	Z	K1A	O5A	Y
Si1	C1	Z	Si1	C2	Y
Si2	C1	Z	Si2	C5	Y
Si3	C1	Z	Si3	C9	Y
Si1A	C1A	Z	Si1A	C2A	Y
Si2A	C1A	Z	Si2A	C5A	Y
Si3A	C1A	Z	Si3A	C9A	Y
Si1B	C1B	Z	Si1B	C3B	Y
Si2B	C1B	Z	Si2B	C7B	Y
Si3B	C1B	Z	Si3B	C8B	Y
Si1C	C1C	Z	Si1C	C3C	Y
Si2C	C1C	Z	Si2C	C7C	Y
Si3C	C1C	Z	Si3C	C8C	Y
O1	C23	X	O1	C37	Y
O2	C29	X	O2	C36	Y
O3	C25	X	O3	C33	Y
O4	C31	X	O4	C32	Y
O5	C21	X	O5	C35	Y
O6	C27	X	O6	C34	Y
O1A	C23A	X	O1A	C37A	Y
O2A	C29A	X	O2A	C36A	Y

O3A	C25A	X	O3A	C33A	Y
O4A	C31A	X	O4A	C32A	Y
O5A	C21A	X	O5A	C35A	Y
O6A	C27A	X	O6A	C34A	Y
N1	K1	Z	N1	C24	Y
N2	K1	Z	N2	C28	Y
N1A	K1A	Z	N1A	C24A	Y
N2A	K1A	Z	N2A	C28A	Y
C1	Fe1	Z	C1	Si1	Y
C2	Si1	Z	C2	H2B	Y
C3	Si1	Z	C3	H3A	Y
C4	Si1	Z	C4	H4B	Y
C5	Si2	Z	C5	H5C	Y
C6	Si2	Z	C6	H6B	Y
C7	Si2	Z	C7	H7B	Y
C8	Si3	Z	C8	H8A	Y
C9	Si3	Z	C9	H9A	Y
C10	Si3	Z	C10	H10A	Y
C1A	Fe1	Z	C1A	Si3A	Y
C2A	Si1A	Z	C2A	H2AA	Y
C3A	Si1A	Z	C3A	H3AC	Y
C4A	Si1A	Z	C4A	H4AB	Y
C5A	Si2A	Z	C5A	H5AC	Y
C6A	Si2A	Z	C6A	H6AC	Y
C7A	Si2A	Z	C7A	H7AA	Y
C8A	Si3A	Z	C8A	H8AB	Y
C9A	Si3A	Z	C9A	H9AB	Y
C10A	Si3A	Z	C10A	H10F	Y
C20	C21	X	C20	N1	Y
C21	C20	X	C21	O5	Y
C22	C23	X	C20	N1	Y

C23	C22	X	C23	O1	Y
C24	C25	X	C20	N1	Y
C25	C24	X	C25	O3	Y
C26	C27	X	C26	N2	Y
C27	C26	X	C27	O6	Y
C28	C29	X	C28	N2	Y
C29	C28	X	C29	O2	Y
C30	C31	X	C30	N2	Y
C31	C30	X	C31	O4	Y
C32	C33	X	C32	O4	Y
C33	C32	X	C33	O3	Y
C34	C35	X	C34	O6	Y
C35	C34	X	C35	O5	Y
C36	C37	X	C36	O2	Y
C37	C36	X	C37	O1	Y
C1B	Fe2	Z	C1B	Si3B	Y
C2B	Si1B	Z	C2B	H2BB	Y
C3B	Si1B	Z	C3B	H3BA	Y
C4B	Si1B	Z	C4B	H4BC	Y
C5B	Si2B	Z	C5B	H5BA	Y
C6B	Si2B	Z	C6B	H6BB	Y
C7B	Si2B	Z	C7B	H7BA	Y
C8B	Si3B	Z	C8B	H8BA	Y
C9B	Si3B	Z	C9B	H9BA	Y
C10B	Si3B	Z	C10B	H10G	Y
C1C	Fe2	Z	C1C	Si2C	Y
C2C	Si1C	Z	C2C	H2CC	Y
C3C	Si1C	Z	C3C	H3CB	Y
C4C	Si1C	Z	C4C	H4CB	Y
C5C	Si2C	Z	C5C	H5CB	Y
C6C	Si2C	Z	C6C	H6CB	Y

C7C	Si2C	Z	C7C	H7CA	Y
C8C	Si3C	Z	C8C	H8CC	Y
C9C	Si3C	Z	C9C	H9CB	Y
C10C	Si3C	Z	C10C	H10K	Y
C20A	C21A	X	C20A	N1A	Y
C21A	C20A	X	C21A	O5A	Y
C22A	C23A	X	C20A	N1A	Y
C23A	C22A	X	C23A	O1A	Y
C24A	C25A	X	C20A	N1A	Y
C25A	C24A	X	C25A	O3A	Y
C26A	C27A	X	C26A	N2A	Y
C27A	C26A	X	C27A	O6A	Y
C28A	C29A	X	C28A	N2A	Y
C29A	C28A	X	C29A	O2A	Y
C30A	C31A	X	C30A	N2A	Y
C31A	C30A	X	C31A	O4A	Y
C32A	C33A	X	C32A	O4A	Y
C33A	C32A	X	C33A	O3A	Y
C34A	C35A	X	C34A	O6A	Y
C35A	C34A	X	C35A	O5A	Y
C36A	C37A	X	C36A	O2A	Y
C37A	C36A	X	C37A	O1A	Y
H2A	C2	Z	H2A	H2B	Y
H2B	C2	Z	H2B	H2A	Y
H2C	C2	Z	H2C	H2A	Y
H3A	C3	Z	H3A	H3B	Y
H3B	C3	Z	H3B	H3A	Y
H3C	C3	Z	H3C	H3B	Y
H4A	C4	Z	H4A	H4B	Y
H4B	C4	Z	H4B	H4C	Y
H4C	C4	Z	H4C	H4B	Y

H5A	C5	Z	H5A	H5C	Y
H5B	C5	Z	H5B	H5C	Y
H5C	C5	Z	H5C	H5A	Y
H6A	C6	Z	H6A	H6B	Y
H6B	C6	Z	H6B	H6A	Y
H6C	C6	Z	H6C	H6A	Y
H7A	C7	Z	H7A	H7C	Y
H7B	C7	Z	H7B	H7A	Y
H7C	C7	Z	H7C	H7A	Y
H8A	C8	Z	H8A	H8C	Y
H8B	C8	Z	H8B	H8A	Y
H8C	C8	Z	H8C	H8A	Y
H9A	C9	Z	H9A	H9B	Y
H9B	C9	Z	H9B	H9A	Y
H9C	C9	Z	H9C	H9B	Y
H10A	C10	Z	H10A	H10C	Y
H10B	C10	Z	H10B	H10C	Y
H10C	C10	Z	H10C	H10B	Y
H2AA	C2A	Z	H2AA	H2AC	Y
H2AB	C2A	Z	H2AB	H2AC	Y
H2AC	C2A	Z	H2AC	H2AB	Y
H3AA	C3A	Z	H3AA	H3AB	Y
H3AB	C3A	Z	H3AB	H3AA	Y
H3AC	C3A	Z	H3AC	H3AB	Y
H4AA	C4A	Z	H4AA	H4AB	Y
H4AB	C4A	Z	H4AB	H4AA	Y
H4AC	C4A	Z	H4AC	H4AA	Y
H5AA	C5A	Z	H5AA	H5AB	Y
H5AB	C5A	Z	H5AB	H5AA	Y
H5AC	C5A	Z	H5AC	H5AA	Y
H6AA	C6A	Z	H6AA	H6AB	Y

H6AB	C6A	Z	H6AB	H6AA	Y
H6AC	C6A	Z	H6AC	H6AB	Y
H7AA	C7A	Z	H7AA	H7AC	Y
H7AB	C7A	Z	H7AB	H7AA	Y
H7AC	C7A	Z	H7AC	H7AA	Y
H8AA	C8A	Z	H8AA	H8AB	Y
H8AB	C8A	Z	H8AB	H8AA	Y
H8AC	C8A	Z	H8AC	H8AB	Y
H9AA	C9A	Z	H9AA	H9AB	Y
H9AB	C9A	Z	H9AB	H9AA	Y
H9AC	C9A	Z	H9AC	H9AA	Y
H10D	C10A	Z	H10D	H10E	Y
H10E	C10A	Z	H10E	H10D	Y
H10F	C10A	Z	H10F	H10D	Y
H20A	C20	Z	H20A	H20B	Y
H20B	C20	Z	H20B	H20A	Y
H21A	C21	Z	H21A	H21B	Y
H21B	C21	Z	H21B	H21A	Y
H22A	C22	Z	H22A	H22B	Y
H22B	C22	Z	H22B	H22A	Y
H23A	C23	Z	H23A	H23B	Y
H23B	C23	Z	H23B	H23A	Y
H24A	C24	Z	H24A	H24B	Y
H24B	C24	Z	H24B	H24A	Y
H25A	C25	Z	H25A	H25B	Y
H25B	C25	Z	H25B	H25A	Y
H26A	C26	Z	H26A	H26B	Y
H26B	C26	Z	H26B	H26A	Y
H27A	C27	Z	H27A	H27B	Y
H27B	C27	Z	H27B	H27A	Y
H28A	C28	Z	H28A	H28B	Y

H28B	C28	Z	H28B	H28A	Y
H29A	C29	Z	H29A	H29B	Y
H29B	C29	Z	H29B	H29A	Y
H30A	C30	Z	H30A	H30B	Y
H30B	C30	Z	H30B	H30A	Y
H31A	C31	Z	H31A	H31B	Y
H31B	C31	Z	H31B	H31A	Y
H32A	C32	Z	H32A	H32B	Y
H32B	C32	Z	H32B	H32A	Y
H33A	C33	Z	H33A	H33B	Y
H33B	C33	Z	H33B	H33A	Y
H34A	C34	Z	H34A	H34B	Y
H34B	C34	Z	H34B	H34A	Y
H35A	C35	Z	H35A	H35B	Y
H35B	C35	Z	H35B	H35A	Y
H36A	C36	Z	H36A	H36B	Y
H36B	C36	Z	H36B	H36A	Y
H37A	C37	Z	H37A	H37B	Y
H37B	C37	Z	H37B	H37A	Y
H2BA	C2B	Z	H2BA	H2BB	Y
H2BB	C2B	Z	H2BB	H2BC	Y
H2BC	C2B	Z	H2BC	H2BB	Y
H3BA	C3B	Z	H3BA	H3BC	Y
H3BB	C3B	Z	H3BB	H3BC	Y
H3BC	C3B	Z	H3BC	H3BA	Y
H4BA	C4B	Z	H4BA	H4BC	Y
H4BB	C4B	Z	H4BB	H4BA	Y
H4BC	C4B	Z	H4BC	H4BA	Y
H5BA	C5B	Z	H5BA	H5BB	Y
H5BB	C5B	Z	H5BB	H5BA	Y
H5BC	C5B	Z	H5BC	H5BA	Y

H6BA	C6B	Z	H6BA	H6BC	Y
H6BB	C6B	Z	H6BB	H6BC	Y
H6BC	C6B	Z	H6BC	H6BB	Y
H7BA	C7B	Z	H7BA	H7BB	Y
H7BB	C7B	Z	H7BB	H7BA	Y
H7BC	C7B	Z	H7BC	H7BA	Y
H8BA	C8B	Z	H8BA	H8BC	Y
H8BB	C8B	Z	H8BB	H8BC	Y
H8BC	C8B	Z	H8BC	H8BB	Y
H9BA	C9B	Z	H9BA	H9BB	Y
H9BB	C9B	Z	H9BB	H9BA	Y
H9BC	C9B	Z	H9BC	H9BB	Y
H10G	C10B	Z	H10G	H10H	Y
H10H	C10B	Z	H10H	H10I	Y
H10I	C10B	Z	H10I	H10H	Y
H2CA	C2C	Z	H2CA	H2CC	Y
H2CB	C2C	Z	H2CB	H2CA	Y
H2CC	C2C	Z	H2CC	H2CA	Y
H3CA	C3C	Z	H3CA	H3CB	Y
H3CB	C3C	Z	H3CB	H3CA	Y
H3CC	C3C	Z	H3CC	H3CA	Y
H4CA	C4C	Z	H4CA	H4CB	Y
H4CB	C4C	Z	H4CB	H4CA	Y
H4CC	C4C	Z	H4CC	H4CA	Y
H5CA	C5C	Z	H5CA	H5CB	Y
H5CB	C5C	Z	H5CB	H5CA	Y
H5CC	C5C	Z	H5CC	H5CA	Y
H6CA	C6C	Z	H6CA	H6CB	Y
H6CB	C6C	Z	H6CB	H6CA	Y
H6CC	C6C	Z	H6CC	H6CA	Y
H7CA	C7C	Z	H7CA	H7CB	Y

H7CB	C7C	Z	H7CB	H7CA	Y
H7CC	C7C	Z	H7CC	H7CB	Y
H8CA	C8C	Z	H8CA	H8CC	Y
H8CB	C8C	Z	H8CB	H8CA	Y
H8CC	C8C	Z	H8CC	H8CA	Y
H9CA	C9C	Z	H9CA	H9CC	Y
H9CB	C9C	Z	H9CB	H9CC	Y
H9CC	C9C	Z	H9CC	H9CB	Y
H10J	C10C	Z	H10J	H10K	Y
H10K	C10C	Z	H10K	H10J	Y
H10L	C10C	Z	H10L	H10J	Y
H20C	C20A	Z	H20C	H20D	Y
H20D	C20A	Z	H20D	H20C	Y
H21C	C21A	Z	H21C	H21D	Y
H21D	C21A	Z	H21D	H21C	Y
H22C	C22A	Z	H22C	H22D	Y
H22D	C22A	Z	H22D	H22C	Y
H23C	C23A	Z	H23C	H23D	Y
H23D	C23A	Z	H23D	H23C	Y
H24C	C24A	Z	H24C	H24D	Y
H24D	C24A	Z	H24D	H24C	Y
H25C	C25A	Z	H25C	H25D	Y
H25D	C25A	Z	H25D	H25C	Y
H26C	C26A	Z	H26C	H26D	Y
H26D	C26A	Z	H26D	H26C	Y
H27C	C27A	Z	H27C	H27D	Y
H27D	C27A	Z	H27D	H27C	Y
H28C	C28A	Z	H28C	H28D	Y
H28D	C28A	Z	H28D	H28C	Y
H29C	C29A	Z	H29C	H29D	Y
H29D	C29A	Z	H29D	H29C	Y

H30C	C30A	Z	H30C	H30D	Y
H30D	C30A	Z	H30D	H30C	Y
H31C	C31A	Z	H31C	H31D	Y
H31D	C31A	Z	H31D	H31C	Y
H32C	C32A	Z	H32C	H32D	Y
H32D	C32A	Z	H32D	H32C	Y
H33C	C33A	Z	H33C	H33D	Y
H33D	C33A	Z	H33D	H33C	Y
H34C	C34A	Z	H34C	H34D	Y
H34D	C34A	Z	H34D	H34C	Y
H35C	C35A	Z	H35C	H35D	Y
H35D	C35A	Z	H35D	H35C	Y
H36C	C36A	Z	H36C	H36D	Y
H36D	C36A	Z	H36D	H36C	Y
H37C	C37A	Z	H37C	H37D	Y
H37D	C37A	Z	H37D	H37C	Y

Table S7. Local atomic right-handed coordinate systems applied in the multipole modelling of compound **2**.

atom	atom0	ax1	atom1	atom2	ax2
Fe1	C1	Z	Fe1	DUMMY ATOM (-0.073,0.041,-0.092)	Y
Si1	C1	Z	Si1	C4	Y
Si2	C1	Z	Si2	C6	Y
Si3	C1	Z	Si3	C8	Y
C1	Fe1	Z	C1	Si3	Y
C7	Si2	Z	C7	H7A	Y
C8	Si3	Z	C8	H8B	Y
C9	Si3	Z	C9	H9B	Y
C3	Si1	Z	C3	H3B	Y
C5	Si2	Z	C5	H5A	Y

C4	Si1	Z	C4	H4C	Y
C2	Si1	Z	C2	H2B	Y
C10	Si3	Z	C10	H10C	Y
C6	Si2	Z	C6	H6C	Y
H7B	C7	Z	H7B	H7A	Y
H7A	C7	Z	H7A	H7B	Y
H7C	C7	Z	H7C	H7A	Y
H8A	C8	Z	H8A	H8B	Y
H8C	C8	Z	H8C	H8B	Y
H8B	C8	Z	H8B	H8A	Y
H9B	C9	Z	H9B	H9A	Y
H9A	C9	Z	H9A	H9B	Y
H9C	C9	Z	H9C	H9B	Y
H3A	C3	Z	H3A	H3B	Y
H3C	C3	Z	H3C	H3B	Y
H3B	C3	Z	H3B	H3A	Y
H5B	C5	Z	H5B	H5A	Y
H5A	C5	Z	H5A	H5B	Y
H5C	C5	Z	H5C	H5A	Y
H4A	C4	Z	H4A	H4C	Y
H4C	C4	Z	H4C	H4B	Y
H4B	C4	Z	H4B	H4C	Y
H2B	C2	Z	H2B	H2C	Y
H2A	C2	Z	H2A	H2C	Y
H2C	C2	Z	H2C	H2B	Y
H10A	C10	Z	H10A	H10C	Y
H10C	C10	Z	H10C	H10A	Y
H10B	C10	Z	H10B	H10A	Y
H6A	C6	Z	H6A	H6B	Y
H6C	C6	Z	H6C	H6A	Y
H6B	C6	Z	H6B	H6A	Y

9. Experimental multipole model parameters

The multipole populations and radial expansion/contraction parameters are provided in Table S8-13 for compound **1** and Table S14-19 for compound **2**. They refer to the local atomic coordinate systems from Table S6 and Table S7.

Table S8. Radial expansion/contraction parameters for the multipole model of compound **1**.These parameters were not refined in the very last refinement. They were instead constrained to values from earlier stages of the refinements. The uncertainty estimates are taken from these earlier refinements.

	κ	$\kappa'_{l=0-4}$
Fe	0.917(2)	0.837(21) ($\kappa'_{l=0}$ is fixed to 1)
Si	1.058(5)	0.815(5)
C1, C1A, C1B, C1C	0.983(5)	0.854(22)
C_{methyl}	0.923(2)	0.779(4)
K	1	1
O	0.976(1)	0.932(12)
N	0.996(3)	0.934(18)
$C_{crypt-222}$	0.955(1)	0.891(3)
H	1.13	1.29

Table S9. Monopole populations and the atomic charges derived from these populations for the multipole model of compound **1**.

	P_v	P_{00}	Net charge from monopole populations
Fe1	6.764(20)	0.814(114)	+0.422(133)
Fe2	6.757(19)	0.810(114)	+0.432(133)
Si	3.103(28)	0	+0.897(28)
C1	4.217(40)	0	-0.216(40)
C1A	4.195(40)	0	-0.194(40)
C1B	4.197(40)	0	-0.196(40)

C1C	4.173(40)	0	-0.172(40)
C_{methyl}	5.289(12)	0	-1.289(12)
H_{methyl}	0.689(4)	0	+0.310(4)
K	0	0	+1
O	6.084(7)	0	-0.084(7)
N	4.921(14)	0	+0.078(14)
$C_{crypt-222}$	4.456(6)	0	-0.456(6)
$H_{crypt-222}$	0.762(3)	0	+0.237(3)

Table S10. Dipole populations for the multipole model of compound **1**.

	P_{11+}	P_{11-}	P_{10}
Fe1	-0.003(7)	-0.030(8)	-0.051(8)
Fe2	0.020(7)	0.012(7)	0.022(8)
Si	0.025(11)	0.021(10)	0.261(15)
C1	0.004(16)	0.029(16)	0.058(18)
C1A	-0.017(16)	-0.009(17)	0.076(18)
C1B	0.017(16)	-0.009(16)	0.077(18)
C1C	0.042(16)	0.013(16)	0.117(18)
C_{methyl}	-0.005(3)	-0.003(3)	-0.020(6)
H_{methyl}	0	0	0.056(2)
K	0	0	0
O	-0.052(3)	-0.080(3)	0.002(3)
N	0	0	0.107(6)
$C_{crypt-222}$	-0.080(3)	-0.101(3)	0.004(3)
$H_{crypt-222}$	0	0	0

Table S11. Quadrupole populations for the multipole model of compound **1**.

	P_{20}	P_{21+}	P_{21-}	P_{22+}	P_{22-}
Fe1	-0.163(11)	-0.002(10)	-0.048(10)	-0.129(10)	0.000(10)
Fe2	-0.194(11)	0.014(10)	-0.038(10)	-0.110(10)	0.002(10)

Si	0.185(13)	-0.009(11)	-0.006(11)	-0.011(9)	0.046(10)
C1	0.009(18)	-0.011(15)	0.024(15)	-0.013(15)	-0.002(15)
C1A	0.017(18)	-0.011(15)	0.032(16)	0.017(15)	-0.001(15)
C1B	0.020(17)	-0.050(15)	0.059(15)	-0.014(15)	0.018(15)
C1C	0.054(17)	-0.021(16)	-0.017(15)	0.018(15)	-0.003(15)
C_{methyl}	0.023(5)	-0.010(3)	0.007(3)	-0.005(3)	-0.014(3)
H_{methyl}	0	0	0	0	0
K	0	0	0	0	0
O	0.130(4)	-0.009(3)	0.016(3)	-0.025(3)	0.049(3)
N	0.108(6)	0	0	0	0
$C_{crypt\text{-}222}$	0.036(3)	0.000(3)	-0.001(3)	0.010(3)	0.062(3)
$H_{crypt\text{-}222}$	0	0	0	0	0

Table S12. Octupole populations for the multipole model of compound **1**.

	P_{30}	P_{31+}	P_{31-}	P_{32+}	P_{32-}	P_{33+}	P_{33-}
Fe1	0.018(12)	0.006(10)	0.032(11)	0.007(11)	0.001(11)	0.017(10)	0.022(10)
Fe2	-0.005(11)	0.011(10)	0.010(11)	-0.006(10)	-0.004(11)	-0.001(10)	0.038(10)
Si	0.446(13)	0.005(10)	-0.009(10)	0.001(9)	-0.009(10)	-0.026(7)	-0.266(11)
C1	0.085(22)	-0.019(20)	0.018(20)	-0.005(20)	-0.011(20)	-0.003(21)	-0.104(20)
C1A	0.075(23)	-0.015(20)	0.003(20)	-0.013(20)	-0.031(20)	0.001(21)	-0.120(20)
C1B	0.086(22)	-0.017(20)	-0.030(20)	0.038(20)	-0.046(20)	-0.001(21)	-0.096(20)
C1C	0.079(22)	-0.007(20)	0.077(20)	0.056(20)	-0.022(20)	-0.035(21)	-0.026(20)
C_{methyl}	0.406(6)	0.004(4)	-0.006(4)	0.009(4)	-0.004(4)	-0.011(4)	-0.242(5)
H_{methyl}	0	0	0	0	0	0	0
K	0	0	0	0	0	0	0
O	-0.002(5)	-0.014(4)	-0.021(4)	-0.001(4)	0.003(4)	0.103(4)	-0.022(4)
N	0.141(9)	0	0	0	0	-0.016(8)	-0.151(8)
$C_{crypt\text{-}222}$	0.017(4)	-0.185(4)	-0.300(4)	0.007(4)	-0.003(3)	0.329(4)	-0.076(4)
$H_{crypt\text{-}222}$	0	0	0	0	0	0	0

Table S13. Hexadecapole populations for the multipole model of compound **1**.

	P_{40}	P_{41+}	P_{41-}	P_{42+}	P_{42-}
Fe1	0.240(20)	-0.062(17)	-0.057(19)	-0.040(18)	-0.024(18)
Fe2	0.271(20)	0.049(17)	-0.052(18)	-0.024(17)	-0.043(18)
Si	0.099(11)	-0.019(10)	-0.003(9)	0.005(9)	0.006(9)
C1	-0.055(29)	-0.009(25)	0.017(25)	0.006(25)	0.041(25)
C1A	0.009(29)	-0.010(25)	-0.026(25)	0.009(25)	-0.003(26)
C1B	-0.017(29)	0.008(25)	-0.006(25)	0.008(25)	0.027(25)
C1C	-0.074(29)	0.021(25)	0.011(24)	0.022(25)	0.038(25)
C_{methyl}	0.052(7)	-0.001(5)	0.001(5)	-0.002(5)	-0.016(5)
H_{methyl}	0	0	0	0	0
K	0	0	0	0	0
O	0	0	0	0	0
N	0	0	0	0	0
$C_{crypt-222}$	0	0	0	0	0
$H_{crypt-222}$	0	0	0	0	0
	P_{43+}	P_{43-}	P_{44+}	P_{44-}	
Fe1	-0.064(18)	-0.043(18)	-0.032(17)	-0.062(16)	
Fe2	0.065(18)	-0.045(17)	-0.070(16)	0.104(16)	
Si	0.001(8)	0.097(11)	0.006(8)	0.000(8)	
C1	-0.045(26)	-0.022(25)	-0.008(23)	0.012(23)	
C1A	0.008(26)	0.023(25)	-0.010(23)	-0.003(23)	
C1B	0.025(26)	-0.054(25)	0.058(23)	-0.001(23)	
C1C	0.013(26)	-0.025(25)	0.000(23)	0.042(23)	
C_{methyl}	0.019(5)	0.088(6)	-0.001(5)	0.009(5)	
H_{methyl}	0	0	0	0	
K	0	0	0	0	
O	0	0	0	0	
N	0	0	0	0	
$C_{crypt-222}$	0	0	0	0	
$H_{crypt-222}$	0	0	0	0	

Table S14. Radial expansion/contraction parameters for the multipole model of compound **2**.

	κ	$\kappa'_{l=0-4}$
Fe	0.965(4)	0.825(28)
Si	1	1
C1	0.937(6)	1
C_{methyl}	0.945(2)	1
H	1.13	1.29

Table S15. Monopole populations and the atomic charges derived from these populations for the multipole model of compound **2**.

	P_v	P_{00}	Net charge from monopole populations
Fe1	6.689(39)	0	+1.676(40)
Si1	3.553(66)	0	+0.812(69)
Si2	3.565(68)	0	+0.715(72)
Si3	3.449(65)	0	+0.809(68)
C1	5.036(71)	0	-1.296(74)
C7	4.955(44)	0	-1.052(46)
C8	4.886(44)	0	-1.129(47)
C9	4.989(45)	0	-1.157(47)
C3	4.898(45)	0	-1.077(47)
C5	4.950(44)	0	-1.153(47)
C4	4.925(45)	0	-1.049(47)
C2	4.850(47)	0	-0.985(49)
C10	4.828(46)	0	-1.005(49)
C6	4.817(45)	0	-0.954(47)
H	0.739(8)	0	+0.284(8)

Table S16. Dipole populations for the multipole model of compound **2**.

	P_{11+}	P_{11-}	P_{10}
Fe1	0.000	0.000	0.000
Si1	-0.123(25)	0.085(24)	-0.024(26)
Si2	-0.041(23)	0.026(24)	0.017(29)
Si3	0.010(29)	-0.019(24)	0.021(25)
C1	-0.010(16)	0.016(15)	0.017(13)
C7	-0.006(15)	-0.030(16)	-0.029(14)
C8	0.009(14)	0.011(16)	-0.010(15)
C9	0.023(14)	-0.008(15)	-0.035(16)
C3	0.021(17)	-0.017(14)	-0.020(15)
C5	0.006(14)	-0.003(17)	-0.024(15)
C4	0.004(16)	0.043(16)	-0.009(14)
C2	0.029(14)	0.022(14)	-0.027(19)
C10	0.045(16)	-0.002(14)	-0.015(17)
C6	0.002(15)	0.020(16)	-0.030(16)
H	0	0	0.035(3)

Table S17. Quadrupole populations for the multipole model of compound **2**.

	P_{20}	P_{21+}	P_{21-}	P_{22+}	P_{22-}
Fe1	-0.261(14)	-0.034(13)	0.152(14)	-0.035(15)	0.042(15)
Si1	-0.007(25)	0.036(25)	0.130(22)	0.036(24)	0.032(24)
Si2	-0.026(29)	-0.038(24)	-0.048(23)	-0.036(21)	-0.001(23)
Si3	-0.058(24)	0.013(23)	-0.104(21)	-0.006(24)	-0.091(24)
C1	-0.036(14)	-0.035(14)	0.002(13)	0.026(15)	0.013(15)
C7	-0.006(15)	0.007(15)	0.026(15)	0.000(16)	0.021(16)
C8	0.023(15)	0.030(14)	0.009(15)	-0.036(16)	-0.003(15)
C9	0.011(16)	-0.031(14)	-0.015(16)	0.023(14)	0.008(14)
C3	0.044(16)	0.005(16)	0.021(14)	-0.047(17)	0.034(16)
C5	0.000(16)	-0.038(14)	-0.009(16)	0.031(16)	-0.012(15)
C4	0.024(16)	0.004(15)	-0.013(14)	-0.010(16)	0.034(17)

C2	0.009(18)	0.032(16)	-0.014(16)	0.003(14)	-0.009(13)
C10	-0.002(18)	0.026(17)	-0.012(15)	0.027(16)	-0.018(15)
C6	0.048(17)	0.005(15)	-0.010(17)	0.010(16)	-0.009(15)
H	0	0	0	0	0

Table S18. Octupole populations for the multipole model of compound **2**.

	P_{30}	P_{31+}	P_{31-}	P_{32+}	P_{32-}	P_{33+}	P_{33-}
Fe1	0	0	0	0	0	0	0
Si1	0.157(24)	-0.037(21)	-0.006(20)	-0.036(22)	-0.053(21)	-0.016(20)	-0.165(20)
Si2	0.160(25)	-0.062(22)	-0.031(22)	-0.002(22)	-0.003(20)	-0.038(19)	-0.125(19)
Si3	0.135(22)	0.054(22)	0.015(19)	0.032(20)	-0.085(21)	-0.023(22)	-0.160(21)
C1	0.114(15)	0.034(15)	-0.003(14)	0.014(15)	0.044(15)	0.011(16)	-0.138(16)
C7	0.267(16)	0.003(16)	-0.004(16)	-0.042(16)	-0.007(16)	-0.018(16)	-0.181(17)
C8	0.215(16)	-0.029(15)	0.027(16)	-0.037(16)	-0.042(16)	-0.026(17)	-0.167(17)
C9	0.282(18)	0.022(16)	0.013(17)	0.015(17)	-0.017(16)	-0.036(15)	-0.158(16)
C3	0.252(18)	0.015(16)	-0.030(14)	-0.015(17)	0.025(15)	-0.008(17)	-0.175(17)
C5	0.273(17)	-0.027(15)	-0.007(16)	-0.011(16)	-0.009(16)	-0.041(16)	-0.174(17)
C4	0.251(17)	-0.029(16)	0.011(15)	-0.031(15)	-0.013(16)	0.021(16)	-0.139(17)
C2	0.286(19)	0.015(17)	0.007(18)	0.016(16)	-0.009(16)	0.022(14)	-0.153(15)
C10	0.248(19)	0.001(18)	-0.021(16)	-0.025(17)	0.001(16)	-0.028(15)	-0.168(16)
C6	0.250(18)	0.001(16)	0.011(17)	-0.052(17)	-0.016(16)	-0.025(16)	-0.162(17)
H	0	0	0	0	0	0	0

Table S19. Hexadecapole populations for the multipole model of compound **2**.

	P_{40}	P_{41+}	P_{41-}	P_{42+}	P_{42-}
Fe1	0.157(14)	0.050(13)	-0.049(13)	0.046(14)	0.001(14)
Si1	0.005(23)	-0.060(22)	0.077(20)	0.069(21)	0.054(21)
Si2	0.018(25)	-0.049(22)	-0.072(22)	0.037(21)	0.000(21)
Si3	0.043(22)	0.034(21)	0.069(19)	-0.024(21)	-0.020(20)
C1	-0.029(20)	0.010(18)	-0.019(17)	0.055(19)	-0.013(19)

C7	0.036(21)	-0.031(20)	0.002(21)	-0.002(20)	0.009(20)
C8	0.020(20)	-0.018(19)	-0.040(20)	-0.007(20)	-0.001(20)
C9	0.019(22)	0.011(20)	-0.020(21)	-0.049(21)	0.015(20)
C3	0.053(21)	-0.004(22)	0.022(19)	0.011(21)	-0.009(19)
C5	0.041(21)	0.014(19)	0.007(21)	-0.039(21)	-0.004(20)
C4	0.017(21)	-0.013(20)	-0.018(19)	-0.010(19)	0.024(20)
C2	-0.009(25)	-0.014(22)	0.029(23)	-0.029(21)	0.022(21)
C10	0.015(23)	0.011(23)	0.010(20)	0.002(22)	0.067(22)
C6	-0.037(23)	0.019(20)	0.051(22)	-0.023(21)	0.011(20)
H	0	0	0	0	0
	P_{43+}	P_{43-}	P_{44+}	P_{44-}	
Fe1	-0.014(14)	0.005(15)	0.021(15)	0.110(14)	
Si1	0.067(21)	0.164(21)	-0.050(19)	0.013(19)	
Si2	0.038(20)	0.174(20)	0.020(18)	-0.030(18)	
Si3	0.059(21)	0.078(20)	-0.013(21)	-0.034(20)	
C1	0.024(20)	0.078(20)	0.020(19)	0.027(20)	
C7	-0.009(20)	0.091(21)	0.000(20)	-0.003(19)	
C8	0.034(20)	0.082(20)	-0.013(20)	-0.062(20)	
C9	0.030(19)	0.066(20)	-0.042(17)	-0.002(18)	
C3	0.016(21)	0.035(21)	0.050(21)	0.021(20)	
C5	0.025(19)	0.058(21)	0.009(20)	-0.008(20)	
C4	-0.033(19)	0.053(20)	0.034(21)	-0.001(21)	
C2	0.010(19)	0.069(19)	-0.022(17)	0.015(17)	
C10	0.034(20)	0.073(20)	0.043(19)	0.005(19)	
C6	0.004(21)	0.113(21)	-0.007(20)	-0.004(19)	
H	0	0	0	0	

10. Experimental electron density topology

A search for bond critical points (BCPs) in the $Fe(C(SiMe_3)_3)_2$ moieties of **1** and **2** reveals a BCP for each covalent bond as well as a few BCPs in between the different methyl groups. There are only two BCPs for

each iron atom. These involve the two neighboring carbon atoms. Hence, the iron atoms in compounds **1** and **2** appear to be truly two-coordinate. Table S20 and Table S21 report topological properties obtained for compounds **1** and **2**, respectively, at intramolecular BCPs positioned between atoms separated by a maximum distance of 2.07 Å.

Table S20. Topological properties obtained from the multipole model of compound **1** at intramolecular BCPs positioned between atoms separated by a maximum distance of 2.07 Å. The estimated errors for ρ(**r**) and $\nabla^2\rho(\mathbf{r})$ have some limitations according to the XD2006 manual[9], and they are likely underestimated.

X-Y Bond Path	$\rho(\mathbf{r})_{BCP}$ [eÅ^{-3}]	$\nabla^2\rho(\mathbf{r})_{BCP}$ [eÅ^{-5}]	d_{X-Y} [Å]	d_{X-BCP} [Å]	d_{Y-BCP} [Å]	ε
Fe1-C1	0.576(11)	5.812(23)	2.0670	1.0658	1.0012	0.13
Fe1-C1A	0.605(11)	5.278(23)	2.0615	1.0576	1.0039	0.06
Fe2-C1B	0.604(10)	5.463(23)	2.0616	1.0599	1.0017	0.06
Fe2-C1C	0.595(10)	5.930(22)	2.0668	1.0573	1.0095	0.19
SI1-C1	0.930(9)	-2.441(18)	1.8625	0.7862	1.0763	0.02
SI1-C2	0.902(3)	0.255(11)	1.8865	0.7616	1.1249	0.02
SI1-C3	0.869(4)	0.431(12)	1.8970	0.7663	1.1307	0.04
SI1-C4	0.892(4)	0.124(11)	1.8895	0.7630	1.1265	0.04
SI2-C1	0.926(9)	-2.640(15)	1.8598	0.7890	1.0708	0.05
SI2-C5	0.894(0)	0.092(0)	1.8936	0.7641	1.1295	0.01
SI2-C6	0.892(0)	0.165(0)	1.8885	0.7625	1.1260	0.04
SI2-C7	0.869(0)	0.425(0)	1.8972	0.7663	1.1310	0.01
SI3-C1	0.926(9)	-2.523(15)	1.8613	0.7878	1.0735	0.05
SI3-C8	0.870(0)	0.481(0)	1.8953	0.7657	1.1297	0.04
SI3-C9	0.899(0)	0.172(0)	1.8897	0.7628	1.1269	0.03
SI3-C10	0.893(0)	0.141(0)	1.8886	0.7627	1.1258	0.06
SI1A-C1A	0.952(9)	-2.670(15)	1.8654	0.7812	1.0842	0.03
SI1A-C2A	0.905(0)	0.293(0)	1.8836	0.7612	1.1224	0.02
SI1A-C3A	0.869(0)	0.421(0)	1.8970	0.7665	1.1305	0.03
SI1A-C4A	0.891(0)	0.103(0)	1.8906	0.7634	1.1271	0.04
SI2A-C1A	0.944(9)	-2.665(15)	1.8603	0.7835	1.0768	0.03
SI2A-C5A	0.903(0)	0.273(0)	1.8851	0.7616	1.1235	0.01

SI2A-C6A	0.893(0)	0.169(0)	1.8877	0.7626	1.1251	0.04
SI2A-C7A	0.865(0)	0.331(0)	1.9012	0.7678	1.1334	0.04
SI3A-C1A	0.919(9)	-2.909(16)	1.8624	0.7941	1.0683	0.05
SI3A-C8A	0.866(0)	0.392(0)	1.8992	0.7669	1.1323	0.01
SI3A-C9A	0.897(0)	0.158(0)	1.8903	0.7630	1.1273	0.02
SI3A-C10A	0.896(0)	0.227(0)	1.8856	0.7616	1.1239	0.05
SI1B-C1B	0.909(9)	-2.456(15)	1.8634	0.7935	1.0699	0.07
SI1B-C2B	0.897(0)	0.187(0)	1.8865	0.7617	1.1248	0.05
SI1B-C3B	0.894(0)	0.157(0)	1.8920	0.7635	1.1285	0.02
SI1B-C4B	0.867(0)	0.446(0)	1.8971	0.7659	1.1312	0.02
SI2B-C1B	0.905(9)	-2.392(16)	1.8582	0.7941	1.0640	0.06
SI2B-C5B	0.896(0)	0.251(0)	1.8851	0.7613	1.1238	0.07
SI2B-C6B	0.869(0)	0.422(0)	1.8975	0.7663	1.1312	0.02
SI2B-C7B	0.902(0)	0.301(0)	1.8847	0.7611	1.1236	0.02
SI3B-C1B	0.937(9)	-2.796(15)	1.8613	0.7863	1.0750	0.08
SI3B-C8B	0.900(0)	0.247(0)	1.8870	0.7622	1.1248	0.01
SI3B-C9B	0.885(0)	-0.031(0)	1.8976	0.7654	1.1323	0.06
SI3B-C10B	0.866(0)	0.369(0)	1.8995	0.7671	1.1324	0.04
SI1C-C1C	0.886(10)	-3.016(17)	1.8576	0.8086	1.0490	0.05
SI1C-C2C	0.886(0)	0.037(0)	1.8944	0.7641	1.1304	0.04
SI1C-C3C	0.897(0)	0.257(0)	1.8881	0.7621	1.1260	0.02
SI1C-C4C	0.868(0)	0.404(0)	1.8982	0.7664	1.1318	0.01
SI2C-C1C	0.898(9)	-2.762(16)	1.8586	0.7999	1.0588	0.08
SI2C-C5C	0.893(0)	0.113(0)	1.8899	0.7629	1.1269	0.05
SI2C-C6C	0.870(0)	0.471(0)	1.8950	0.7657	1.1293	0.01
SI2C-C7C	0.897(0)	0.228(0)	1.8885	0.7621	1.1264	0.02
SI3C-C1C	0.894(9)	-2.530(16)	1.8602	0.7998	1.0604	0.09
SI3C-C8C	0.899(0)	0.258(0)	1.8873	0.7620	1.1253	0.01
SI3C-C9C	0.891(0)	0.119(0)	1.8908	0.7630	1.1279	0.05
SI3C-C10C	0.868(0)	0.445(0)	1.8966	0.7658	1.1308	0.01
O1-C23	1.883(3)	-16.372(4)	1.4227	0.8438	0.5789	0.10

O1-C37	1.884(5)	-16.321(15)	1.4236	0.8444	0.5793	0.10
O2-C29	1.889(0)	-16.681(0)	1.4202	0.8442	0.5760	0.10
O2-C36	1.897(0)	-17.067(0)	1.4184	0.8460	0.5724	0.10
O3-C25	1.903(0)	-17.360(0)	1.4155	0.8460	0.5695	0.10
O3-C33	1.893(0)	-16.794(0)	1.4203	0.8455	0.5748	0.10
O4-C31	1.901(0)	-17.305(0)	1.4159	0.8458	0.5701	0.10
O4-C32	1.880(0)	-16.166(0)	1.4248	0.8441	0.5807	0.10
O5-C21	1.881(0)	-16.236(0)	1.4234	0.8433	0.5801	0.10
O5-C35	1.888(0)	-16.613(0)	1.4218	0.8451	0.5767	0.10
O6-C27	1.879(0)	-16.153(0)	1.4243	0.8432	0.5810	0.10
O6-C34	1.878(0)	-16.110(0)	1.4254	0.8441	0.5814	0.10
O1A-C23A	1.879(0)	-16.175(0)	1.4240	0.8433	0.5807	0.10
O1A-C37A	1.895(0)	-16.981(0)	1.4191	0.8459	0.5733	0.10
O2A-C29A	1.882(0)	-16.377(0)	1.4228	0.8438	0.5790	0.10
O2A-C36A	1.888(0)	-16.613(0)	1.4217	0.8450	0.5766	0.10
O3A-C25A	1.892(0)	-16.811(0)	1.4195	0.8447	0.5748	0.10
O3A-C33A	1.890(0)	-16.664(0)	1.4211	0.8451	0.5760	0.10
O4A-C31A	1.895(0)	-16.966(0)	1.4183	0.8450	0.5733	0.10
O4A-C32A	1.900(0)	-17.228(0)	1.4172	0.8464	0.5708	0.10
O5A-C21A	1.877(0)	-16.067(0)	1.4250	0.8431	0.5819	0.10
O5A-C35A	1.876(0)	-15.973(0)	1.4263	0.8437	0.5826	0.10
O6A-C27A	1.883(0)	-16.354(0)	1.4227	0.8436	0.5791	0.10
O6A-C34A	1.892(0)	-16.774(0)	1.4204	0.8453	0.5750	0.10
N1-C20	1.821(5)	-14.017(9)	1.4694	0.8287	0.6407	0.08
N1-C22	1.973(5)	-12.617(11)	1.4692	0.7938	0.6753	0.14
N1-C24	1.568(5)	-1.791(9)	1.4761	0.8220	0.6541	1.17
N2-C26	1.817(0)	-13.896(0)	1.4718	0.8297	0.6421	0.08
N2-C28	1.818(0)	-13.911(0)	1.4717	0.8297	0.6420	0.07
N2-C30	1.814(0)	-13.790(0)	1.4729	0.8299	0.6431	0.07
N1A-C20A	1.820(0)	-13.900(0)	1.4707	0.8294	0.6413	0.08
N1A-C22A	1.730(0)	-5.938(0)	1.4867	0.8040	0.6827	0.30

N1A-C24A	1.938(0)	-11.828(0)	1.4757	0.7952	0.6806	0.10
N2A-C26A	1.816(0)	-13.851(0)	1.4718	0.8297	0.6421	0.07
N2A-C28A	1.827(0)	-14.186(0)	1.4682	0.8295	0.6388	0.08
N2A-C30A	1.820(0)	-13.985(0)	1.4704	0.8298	0.6406	0.08
C2-H2A	1.663(8)	-16.194(30)	1.0663	0.7484	0.3179	0.03
C2-H2B	1.662(2)	-16.337(7)	1.0661	0.7468	0.3193	0.03
C2-H2C	1.656(2)	-16.104(7)	1.0661	0.7459	0.3203	0.04
C3-H3A	1.665(0)	-16.382(0)	1.0660	0.7467	0.3193	0.03
C3-H3B	1.655(0)	-16.182(0)	1.0661	0.7452	0.3209	0.03
C3-H3C	1.665(0)	-16.283(0)	1.0661	0.7480	0.3181	0.03
C4-H4A	1.668(0)	-16.339(0)	1.0660	0.7482	0.3178	0.04
C4-H4B	1.662(0)	-16.362(0)	1.0661	0.7467	0.3194	0.03
C4-H4C	1.660(0)	-16.191(0)	1.0660	0.7456	0.3204	0.03
C5-H5A	1.651(0)	-15.963(0)	1.0664	0.7462	0.3201	0.04
C5-H5B	1.660(0)	-16.152(0)	1.0664	0.7487	0.3177	0.03
C5-H5C	1.663(0)	-16.265(0)	1.0662	0.7473	0.3189	0.04
C6-H6A	1.664(0)	-16.250(0)	1.0662	0.7485	0.3177	0.04
C6-H6B	1.662(0)	-16.343(0)	1.0661	0.7468	0.3193	0.03
C6-H6C	1.657(0)	-16.167(0)	1.0661	0.7455	0.3206	0.03
C7-H7A	1.662(0)	-16.232(0)	1.0662	0.7481	0.3181	0.03
C7-H7B	1.662(0)	-16.338(0)	1.0661	0.7467	0.3195	0.03
C7-H7C	1.656(0)	-16.152(0)	1.0661	0.7455	0.3205	0.03
C8-H8A	1.665(0)	-16.383(0)	1.0660	0.7467	0.3194	0.03
C8-H8B	1.646(0)	-15.916(0)	1.0666	0.7459	0.3207	0.03
C8-H8C	1.662(0)	-16.222(0)	1.0662	0.7481	0.3181	0.04
C9-H9A	1.666(0)	-16.388(0)	1.0660	0.7468	0.3192	0.03
C9-H9B	1.655(0)	-16.144(0)	1.0661	0.7456	0.3205	0.03
C9-H9C	1.669(0)	-16.331(0)	1.0660	0.7484	0.3177	0.03
C10-H10A	1.662(0)	-16.265(0)	1.0662	0.7472	0.3190	0.04
C10-H10B	1.651(0)	-16.040(0)	1.0662	0.7459	0.3204	0.04
C10-H10C	1.665(0)	-16.203(0)	1.0663	0.7486	0.3177	0.03

C2A-H2AA	1.666(0)	-16.370(0)	1.0660	0.7470	0.3191	0.04
C2A-H2AB	1.652(0)	-16.082(0)	1.0662	0.7457	0.3205	0.03
C2A-H2AC	1.661(0)	-16.098(0)	1.0664	0.7488	0.3176	0.03
C3A-H3AA	1.657(0)	-16.185(0)	1.0660	0.7454	0.3206	0.03
C3A-H3AB	1.662(0)	-16.272(0)	1.0662	0.7480	0.3182	0.03
C3A-H3AC	1.665(0)	-16.380(0)	1.0660	0.7466	0.3194	0.03
C4A-H4AA	1.667(0)	-16.349(0)	1.0660	0.7480	0.3180	0.04
C4A-H4AB	1.661(0)	-16.341(0)	1.0661	0.7468	0.3194	0.03
C4A-H4AC	1.658(0)	-16.153(0)	1.0661	0.7455	0.3206	0.03
C5A-H5AA	1.653(0)	-16.030(0)	1.0663	0.7461	0.3202	0.04
C5A-H5AB	1.655(0)	-16.040(0)	1.0667	0.7488	0.3179	0.02
C5A-H5AC	1.666(0)	-16.372(0)	1.0660	0.7470	0.3191	0.03
C6A-H6AA	1.654(0)	-16.050(0)	1.0662	0.7460	0.3202	0.04
C6A-H6AB	1.660(0)	-16.202(0)	1.0663	0.7484	0.3179	0.03
C6A-H6AC	1.667(0)	-16.388(0)	1.0660	0.7468	0.3192	0.03
C7A-H7AA	1.664(0)	-16.372(0)	1.0660	0.7466	0.3194	0.03
C7A-H7AB	1.656(0)	-16.181(0)	1.0660	0.7454	0.3206	0.03
C7A-H7AC	1.667(0)	-16.336(0)	1.0660	0.7481	0.3180	0.04
C8A-H8AA	1.664(0)	-16.294(0)	1.0661	0.7480	0.3181	0.03
C8A-H8AB	1.662(0)	-16.339(0)	1.0661	0.7467	0.3194	0.03
C8A-H8AC	1.657(0)	-16.170(0)	1.0660	0.7455	0.3206	0.03
C9A-H9AA	1.663(0)	-16.191(0)	1.0663	0.7486	0.3177	0.04
C9A-H9AB	1.659(0)	-16.238(0)	1.0664	0.7472	0.3192	0.02
C9A-H9AC	1.654(0)	-16.029(0)	1.0663	0.7463	0.3200	0.04
C10A-H10D	1.656(0)	-16.147(0)	1.0661	0.7457	0.3204	0.03
C10A-H10E	1.657(0)	-16.134(0)	1.0665	0.7484	0.3181	0.03
C10A-H10F	1.666(0)	-16.353(0)	1.0661	0.7469	0.3192	0.03
C20-C21	1.809(0)	-16.417(0)	1.5109	0.7559	0.7550	0.06
C20-H20A	1.566(0)	-12.585(0)	1.0924	0.7783	0.3142	0.05
C20-H20B	1.571(0)	-12.666(0)	1.0921	0.7788	0.3133	0.06
C21-H21A	1.561(0)	-12.509(0)	1.0926	0.7784	0.3143	0.04

C21-H21B	1.568(0)	-12.663(0)	1.0921	0.7784	0.3138	0.05
C22-C23	1.802(0)	-16.251(0)	1.5138	0.7575	0.7563	0.08
C22-H22A	1.449(0)	-11.676(0)	1.0930	0.7554	0.3375	0.00
C22-H22B	1.561(0)	-12.530(0)	1.0927	0.7783	0.3144	0.04
C23-H23A	1.568(0)	-12.682(0)	1.0921	0.7781	0.3141	0.05
C23-H23B	1.569(0)	-12.643(0)	1.0922	0.7787	0.3135	0.05
C24-C25	1.811(0)	-16.470(0)	1.5098	0.7555	0.7543	0.09
C24-H24A	1.302(0)	-4.852(0)	1.0999	0.7670	0.3329	0.56
C24-H24B	1.157(0)	-2.096(0)	1.0974	0.7410	0.3564	0.74
C25-H25A	1.562(0)	-12.485(0)	1.0927	0.7786	0.3140	0.05
C25-H25B	1.571(0)	-12.670(0)	1.0920	0.7786	0.3135	0.06
C26-C27	1.801(0)	-16.249(0)	1.5140	0.7575	0.7565	0.05
C26-H26A	1.564(0)	-12.549(0)	1.0925	0.7783	0.3143	0.04
C26-H26B	1.569(0)	-12.620(0)	1.0922	0.7788	0.3134	0.07
C27-H27A	1.566(0)	-12.607(0)	1.0923	0.7783	0.3140	0.05
C27-H27B	1.567(0)	-12.638(0)	1.0922	0.7784	0.3138	0.04
C28-C29	1.814(0)	-16.514(0)	1.5090	0.7549	0.7541	0.06
C28-H28A	1.560(0)	-12.448(0)	1.0928	0.7782	0.3146	0.04
C28-H28B	1.568(0)	-12.611(0)	1.0922	0.7788	0.3134	0.07
C29-H29A	1.567(0)	-12.651(0)	1.0922	0.7783	0.3139	0.05
C29-H29B	1.566(0)	-12.622(0)	1.0923	0.7784	0.3139	0.05
C30-C31	1.799(0)	-16.207(0)	1.5147	0.7577	0.7570	0.05
C30-H30A	1.565(0)	-12.583(0)	1.0924	0.7782	0.3142	0.04
C30-H30B	1.568(0)	-12.611(0)	1.0922	0.7788	0.3135	0.06
C31-H31A	1.564(0)	-12.578(0)	1.0924	0.7782	0.3142	0.04
C31-H31B	1.568(0)	-12.666(0)	1.0921	0.7784	0.3138	0.05
C32-C33	1.844(0)	-17.247(0)	1.4961	0.7481	0.7480	0.07
C32-H32A	1.565(0)	-12.645(0)	1.0923	0.7782	0.3141	0.04
C32-H32B	1.570(0)	-12.674(0)	1.0921	0.7786	0.3135	0.05
C33-H33A	1.566(0)	-12.658(0)	1.0923	0.7783	0.3140	0.04
C33-H33B	1.571(0)	-12.686(0)	1.0920	0.7787	0.3133	0.05

C34-C35	1.826(0)	-16.828(0)	1.5034	0.7517	0.7518	0.06
C34-H34A	1.564(0)	-12.627(0)	1.0924	0.7781	0.3142	0.04
C34-H34B	1.570(0)	-12.683(0)	1.0921	0.7785	0.3135	0.05
C35-H35A	1.563(0)	-12.598(0)	1.0924	0.7781	0.3143	0.04
C35-H35B	1.570(0)	-12.693(0)	1.0920	0.7786	0.3134	0.05
C36-C37	1.842(2)	-17.207(6)	1.4968	0.7484	0.7484	0.07
C36-H36A	1.566(0)	-12.655(0)	1.0923	0.7782	0.3140	0.05
C36-H36B	1.571(0)	-12.679(0)	1.0920	0.7788	0.3133	0.06
C37-H37A	1.562(3)	-12.590(6)	1.0925	0.7782	0.3143	0.04
C37-H37B	1.570(3)	-12.681(6)	1.0921	0.7786	0.3134	0.05
C2B-H2BA	1.665(0)	-16.272(0)	1.0662	0.7482	0.3180	0.03
C2B-H2BB	1.660(0)	-16.285(0)	1.0663	0.7470	0.3193	0.03
C2B-H2BC	1.658(0)	-16.182(0)	1.0660	0.7455	0.3205	0.03
C3B-H3BA	1.665(0)	-16.348(0)	1.0661	0.7469	0.3192	0.04
C3B-H3BB	1.656(0)	-16.185(0)	1.0660	0.7455	0.3206	0.03
C3B-H3BC	1.669(0)	-16.335(0)	1.0660	0.7483	0.3177	0.03
C4B-H4BA	1.657(0)	-16.162(0)	1.0660	0.7456	0.3205	0.03
C4B-H4BB	1.661(0)	-16.236(0)	1.0663	0.7480	0.3182	0.03
C4B-H4BC	1.664(0)	-16.385(0)	1.0660	0.7466	0.3194	0.03
C5B-H5BA	1.665(0)	-16.383(0)	1.0660	0.7467	0.3193	0.03
C5B-H5BB	1.651(0)	-16.067(0)	1.0664	0.7457	0.3207	0.02
C5B-H5BC	1.668(0)	-16.350(0)	1.0660	0.7481	0.3179	0.03
C6B-H6BA	1.658(0)	-16.094(0)	1.0665	0.7484	0.3180	0.03
C6B-H6BB	1.663(0)	-16.363(0)	1.0661	0.7467	0.3194	0.03
C6B-H6BC	1.655(0)	-16.141(0)	1.0661	0.7455	0.3206	0.03
C7B-H7BA	1.667(0)	-16.385(0)	1.0660	0.7470	0.3190	0.03
C7B-H7BB	1.656(0)	-16.185(0)	1.0660	0.7454	0.3206	0.03
C7B-H7BC	1.665(0)	-16.226(0)	1.0662	0.7484	0.3178	0.03
C8B-H8BA	1.665(0)	-16.387(0)	1.0660	0.7466	0.3194	0.03
C8B-H8BB	1.655(0)	-16.160(0)	1.0661	0.7455	0.3206	0.03
C8B-H8BC	1.669(0)	-16.348(0)	1.0660	0.7483	0.3177	0.04

C9B-H9BA	1.663(0)	-16.358(0)	1.0661	0.7467	0.3194	0.04
C9B-H9BB	1.641(0)	-15.808(0)	1.0669	0.7462	0.3207	0.01
C9B-H9BC	1.668(0)	-16.342(0)	1.0660	0.7480	0.3180	0.03
C10B-H10G	1.665(0)	-16.345(0)	1.0661	0.7469	0.3192	0.04
C10B-H10H	1.656(0)	-16.193(0)	1.0660	0.7453	0.3207	0.03
C10B-H10I	1.666(0)	-16.310(0)	1.0661	0.7481	0.3180	0.03
C2C-H2CA	1.654(0)	-16.067(0)	1.0662	0.7459	0.3203	0.04
C2C-H2CB	1.660(0)	-16.198(0)	1.0664	0.7484	0.3179	0.03
C2C-H2CC	1.666(0)	-16.383(0)	1.0660	0.7467	0.3193	0.03
C3C-H3CA	1.662(0)	-16.191(0)	1.0663	0.7484	0.3179	0.03
C3C-H3CB	1.663(0)	-16.375(0)	1.0661	0.7467	0.3193	0.03
C3C-H3CC	1.659(0)	-16.178(0)	1.0660	0.7456	0.3204	0.03
C4C-H4CA	1.666(0)	-16.329(0)	1.0660	0.7479	0.3181	0.03
C4C-H4CB	1.663(0)	-16.357(0)	1.0661	0.7467	0.3194	0.03
C4C-H4CC	1.657(0)	-16.181(0)	1.0660	0.7454	0.3206	0.03
C5C-H5CA	1.664(0)	-16.237(0)	1.0662	0.7484	0.3178	0.04
C5C-H5CB	1.660(0)	-16.263(0)	1.0663	0.7472	0.3191	0.02
C5C-H5CC	1.658(0)	-16.165(0)	1.0660	0.7457	0.3204	0.03
C6C-H6CA	1.664(0)	-16.249(0)	1.0662	0.7482	0.3180	0.03
C6C-H6CB	1.663(0)	-16.369(0)	1.0661	0.7467	0.3194	0.03
C6C-H6CC	1.656(0)	-16.142(0)	1.0661	0.7456	0.3205	0.03
C7C-H7CA	1.666(0)	-16.386(0)	1.0660	0.7468	0.3192	0.03
C7C-H7CB	1.657(0)	-16.198(0)	1.0660	0.7455	0.3205	0.03
C7C-H7CC	1.669(0)	-16.344(0)	1.0660	0.7483	0.3178	0.03
C8C-H8CA	1.659(0)	-16.172(0)	1.0660	0.7457	0.3203	0.03
C8C-H8CB	1.660(0)	-16.194(0)	1.0664	0.7484	0.3180	0.03
C8C-H8CC	1.666(0)	-16.341(0)	1.0661	0.7471	0.3190	0.04
C9C-H9CA	1.662(0)	-16.225(0)	1.0662	0.7483	0.3179	0.04
C9C-H9CB	1.656(0)	-16.149(0)	1.0666	0.7475	0.3191	0.02
C9C-H9CC	1.656(0)	-16.141(0)	1.0661	0.7455	0.3206	0.03
C10C-H10J	1.664(0)	-16.262(0)	1.0661	0.7481	0.3181	0.03

C10C-H10K	1.662(0)	-16.330(0)	1.0661	0.7468	0.3194	0.03
C10C-H10L	1.657(0)	-16.189(0)	1.0660	0.7453	0.3207	0.03
C20A-C21A	1.800(0)	-16.220(0)	1.5145	0.7578	0.7566	0.06
C20A-H20C	1.564(0)	-12.567(0)	1.0925	0.7783	0.3142	0.05
C20A-H20D	1.571(0)	-12.644(0)	1.0921	0.7786	0.3135	0.05
C21A-H21C	1.565(0)	-12.651(0)	1.0923	0.7781	0.3141	0.04
C21A-H21D	1.568(0)	-12.584(0)	1.0923	0.7787	0.3136	0.06
C22A-C23A	1.811(0)	-16.482(0)	1.5096	0.7553	0.7543	0.11
C22A-H22C	1.231(0)	-5.039(0)	1.1015	0.7512	0.3503	0.40
C22A-H22D	1.368(0)	-6.943(0)	1.1021	0.7762	0.3259	0.33
C23A-H23C	1.564(0)	-12.585(0)	1.0924	0.7781	0.3143	0.04
C23A-H23D	1.566(0)	-12.556(0)	1.0924	0.7788	0.3136	0.06
C24A-C25A	1.807(0)	-16.394(0)	1.5114	0.7559	0.7555	0.08
C24A-H24C	1.571(0)	-12.681(0)	1.0921	0.7787	0.3134	0.06
C24A-H24D	1.449(0)	-11.634(0)	1.0931	0.7556	0.3375	0.03
C25A-H25C	1.564(0)	-12.589(0)	1.0924	0.7781	0.3144	0.04
C25A-H25D	1.569(0)	-12.645(0)	1.0921	0.7785	0.3136	0.05
C26A-C27A	1.811(0)	-16.453(0)	1.5101	0.7553	0.7547	0.07
C26A-H26C	1.567(0)	-12.665(0)	1.0922	0.7784	0.3138	0.06
C26A-H26D	1.569(0)	-12.590(0)	1.0923	0.7786	0.3136	0.05
C27A-H27C	1.556(0)	-12.455(0)	1.0928	0.7780	0.3148	0.04
C27A-H27D	1.570(0)	-12.657(0)	1.0921	0.7786	0.3135	0.06
C28A-C29A	1.808(0)	-16.402(0)	1.5112	0.7561	0.7551	0.07
C28A-H28C	1.567(0)	-12.652(0)	1.0923	0.7784	0.3138	0.06
C28A-H28D	1.568(0)	-12.582(0)	1.0923	0.7786	0.3137	0.04
C29A-H29C	1.568(0)	-12.703(0)	1.0921	0.7782	0.3139	0.05
C29A-H29D	1.571(0)	-12.661(0)	1.0920	0.7786	0.3134	0.06
C30A-C31A	1.799(0)	-16.205(0)	1.5148	0.7580	0.7568	0.07
C30A-H30C	1.562(0)	-12.527(0)	1.0926	0.7785	0.3141	0.06
C30A-H30D	1.570(0)	-12.630(0)	1.0922	0.7787	0.3135	0.05
C31A-H31C	1.565(0)	-12.651(0)	1.0923	0.7781	0.3142	0.04

C31A-H31D	1.562(0)	-12.446(0)	1.0927	0.7788	0.3139	0.05
C32A-C33A	1.832(0)	-16.992(0)	1.5007	0.7504	0.7503	0.06
C32A-H32C	1.567(0)	-12.657(0)	1.0922	0.7783	0.3139	0.04
C32A-H32D	1.569(0)	-12.679(0)	1.0921	0.7785	0.3136	0.05
C33A-H33C	1.567(0)	-12.655(0)	1.0923	0.7782	0.3140	0.04
C33A-H33D	1.570(0)	-12.679(0)	1.0921	0.7786	0.3134	0.05
C34A-C35A	1.836(0)	-17.081(0)	1.4992	0.7497	0.7495	0.05
C34A-H34C	1.568(0)	-12.691(0)	1.0921	0.7784	0.3137	0.05
C34A-H34D	1.566(0)	-12.596(0)	1.0923	0.7785	0.3138	0.04
C35A-H35C	1.566(0)	-12.632(0)	1.0923	0.7783	0.3140	0.04
C35A-H35D	1.570(0)	-12.696(0)	1.0920	0.7786	0.3134	0.06
C36A-C37A	1.832(0)	-16.967(0)	1.5010	0.7505	0.7504	0.05
C36A-H36C	1.567(0)	-12.677(0)	1.0922	0.7782	0.3140	0.04
C36A-H36D	1.565(0)	-12.608(0)	1.0923	0.7784	0.3139	0.05
C37A-H37C	1.567(0)	-12.679(0)	1.0922	0.7782	0.3140	0.05
C37A-H37D	1.568(0)	-12.656(0)	1.0922	0.7785	0.3137	0.04

Table S21. Topological properties obtained from the multipole model of compound **2** at intramolecular BCPs positioned between atoms separated by a maximum distance of 2.07 Å. The estimated errors for $\rho(\mathbf{r})$ and $\nabla^2\rho(\mathbf{r})$ have some limitations according to the XD2006 manual[9], and they are likely underestimated.

X-Y Bond Path	$\rho(\mathbf{r})_{BCP}$ [eÅ^{-3}]	$\nabla^2\rho(\mathbf{r})_{BCP}$ [eÅ^{-5}]	d_{X-Y} [Å]	d_{X-BCP} [Å]	d_{Y-BCP} [Å]	ε
Fe1-C1	0.539(13)	6.855(23)	2.0537	1.0217	1.0319	0.17
Si1-C1	0.757(27)	0.974(84)	1.8931	0.7737	1.1194	0.38
Si1-C3	0.792(26)	1.531(87)	1.8863	0.7507	1.1356	0.53
Si1-C4	0.837(25)	-0.241(84)	1.8849	0.7576	1.1273	0.40
Si1-C2	0.986(27)	-5.152(90)	1.8869	0.7735	1.1134	0.15
Si2-C1	0.793(28)	0.130(90)	1.8960	0.7725	1.1235	0.24
Si2-C7	0.849(25)	-0.648(82)	1.8797	0.7556	1.1241	0.07
Si2-C5	0.868(26)	-0.987(85)	1.8839	0.7546	1.1293	0.17

Si2-C6	0.850(26)	-0.866(83)	1.8870	0.7679	1.1191	0.32
Si3-C1	0.763(26)	1.958(83)	1.8862	0.7594	1.1268	0.47
Si3-C8	0.872(25)	-1.420(81)	1.8843	0.7645	1.1199	0.18
Si3-C9	0.810(26)	1.248(87)	1.8909	0.7583	1.1326	0.36
Si3-C10	0.762(27)	2.412(89)	1.8827	0.7584	1.1243	0.02
C7-H7B	1.669(28)	-17.028(79)	1.0661	0.7715	0.2945	0.02
C7-H7A	1.626(28)	-16.196(87)	1.0660	0.7625	0.3035	0.01
C7-H7C	1.731(27)	-18.917(79)	1.0662	0.7807	0.2855	0.04
C8-H8A	1.655(27)	-16.659(81)	1.0668	0.7706	0.2963	0.09
C8-H8C	1.653(27)	-17.108(79)	1.0664	0.7654	0.3010	0.03
C8-H8B	1.623(27)	-15.030(82)	1.0671	0.7705	0.2966	0.06
C9-H9B	1.645(26)	-15.873(81)	1.0671	0.7724	0.2947	0.06
C9-H9A	1.671(27)	-17.131(78)	1.0661	0.7712	0.2949	0.03
C9-H9C	1.698(27)	-17.637(78)	1.0664	0.7773	0.2891	0.03
C3-H3A	1.611(28)	-14.896(87)	1.0664	0.7668	0.2996	0.02
C3-H3C	1.585(29)	-14.020(86)	1.0669	0.7630	0.3039	0.04
C3-H3B	1.662(28)	-17.120(83)	1.0670	0.7712	0.2958	0.01
C5-H5B	1.706(28)	-17.647(80)	1.0663	0.7801	0.2862	0.05
C5-H5A	1.644(29)	-16.163(100)	1.0671	0.7699	0.2972	0.02
C5-H5C	1.648(27)	-16.103(79)	1.0662	0.7701	0.2961	0.03
C4-H4A	1.587(29)	-14.854(85)	1.0667	0.7588	0.3080	0.06
C4-H4C	1.637(27)	-15.629(81)	1.0661	0.7695	0.2966	0.03
C4-H4B	1.629(28)	-15.951(85)	1.0661	0.7659	0.3003	0.06
C2-H2B	1.673(27)	-17.236(79)	1.0665	0.7731	0.2934	0.09
C2-H2A	1.622(27)	-16.150(80)	1.0674	0.7650	0.3024	0.00
C2-H2C	1.616(28)	-15.436(84)	1.0662	0.7644	0.3018	0.02
C10-H10A	1.668(28)	-16.719(82)	1.0660	0.7731	0.2929	0.04
C10-H10C	1.645(28)	-17.019(83)	1.0661	0.7643	0.3018	0.07
C10-H10B	1.616(29)	-15.830(86)	1.0679	0.7670	0.3009	0.04
C6-H6A	1.646(28)	-17.053(83)	1.0666	0.7656	0.3010	0.03
C6-H6C	1.632(29)	-16.572(89)	1.0676	0.7655	0.3021	0.04

C6-H6B	1.649(28)	-17.089(82)	1.0666	0.7667	0.2999	0.02

11. Experimental atomic charges for iron

The atomic charges for iron in **1** and **2** have been determined from integration of the experimental multipole model electron density within the atomic basins determined according to Bader's Quantum Theory of Atoms in Molecules[19] (QTAIM). Table S22 reports these iron charges for both compounds. The charges confirm that iron is more positive in **2** than in **1**, although the values deviate somewhat from the formal oxidations states of +1 in **1** and +2 in **2**. The Langrangian has been integrated in the atomic basins as well. This value should be zero and thereby serves as a measure of the accuracy of the integration.

Table S22. Atomic iron charges, Q_{QTAIM}, and absolute Lagrangian values, |L|, for **1** and **2**.

		Q_{QTAIM}	**|L| [a.u.]**
1	Fe1	+0.59	$9.49 \cdot 10^{-5}$
	Fe2	+0.60	$1.08 \cdot 10^{-5}$
2	Fe1	+1.40	$1.63 \cdot 10^{-5}$

12. References

1. *CrysAlisPro*, 1.171.37.31; Agilent Technologies: 2014.
2. Blessing, R. H., Data Reduction and Error Analysis for Accurate Single Crystal Diffraction Intensities. *Crystallography Reviews* **1987,** *1*, 3-58.
3. Blessing, R. H., DREADD - data reduction and error analysis for single-crystal diffractometer data. . *J. Appl. Crystallogr.* **1989,** *22*, 396-397.
4. Zadrozny, J. M.; Xiao, D. J.; Atanasov, M.; Long, G. J.; Grandjean, F.; Neese, F.; Long, J. R., Magnetic blocking in a linear iron(I) complex. *Nat Chem* **2013,** *5*, 577-581.
5. *RAPID-AUTO*, Rigaku Corporation: Tokyo, Japan, 2004.
6. Sheldrick, G., SHELXT - Integrated space-group and crystal-structure determination. *Acta Crystallogr. Sect. A* **2015,** *71*, 3-8.
7. Dolomanov, O. V.; Bourhis, L. J.; Gildea, R. J.; Howard, J. A. K.; Puschmann, H., OLEX2: a complete structure solution, refinement and analysis program. *J. Appl. Crystallogr.* **2009,** *42*, 339-341.
8. Sheldrick, G. M., A short history of SHELX. *Acta Crystallogr. Sect. A* **2008,** *64*, 112-22.
9. Volkov, A.; Macchi, P.; Farrugia, L. J.; Gatti, C.; Mallinson, P. R.; Richter, T.; Koritsanszky, T. *XD2006 - a computer program for multipole refinement, topological analysis and evaluation of intermolecular*

energies from experimental and theoretical structure factors., revision 5.34; University at Buffalo, State University of New York, Buffalo, NY, University of Milano, Milano, Italy, University of Glasgow, Glasgow, U.K., CNRISTM, Milano, Italy, and Middle Tennessee State University Murfreesboro, TN, 2006.

10. Hansen, N. K.; Coppens, P., Electron Population Analysis of Accurate Diffraction Data. VI. Testing Aspherical Atom Refinements on Small-Molecule Data Sets. *Acta Crystallographica, Section A* **1978,** *34*, 909-921.

11. Su, Z. W.; Coppens, P., Nonlinear Least-Squares Fitting of Numerical Relativistic Atomic Wave Functions by a Linear Combination of Slater-Type Functions for Atoms with Z = 1-36. *Acta Crystallographica, Section A* **1998,** *54*, 646-652.

12. Su, Z. W.; Coppens, P., Relativistic X-ray Elastic Scattering Factors for Neutral Atoms Z=1-54 from Multi-configuration Dirac-Fock Wavefunctions in the 0-12 $Å^{-1}$ sin θ/λ Range, and Six-Gaussian Analytical Expressions in the 0-6 $Å^{-1}$ Range. *Acta Crystallographica, Section A* **1997,** *53*, 749-762.

13. Macchi, P.; Coppens, P., Relativistic analytical wave functions and scattering factors for neutral atoms beyond Kr and for all chemically important ions up to I^-. *Acta Crystallographica, Section A* **2001,** *57*, 656-662.

14. Allen, F. H.; Kennard, O.; Watson, D. G.; Brammer, L.; Orpen, A. G.; Taylor, R., Tables of Bond Lengths determined by X-Ray and Neutron Diffraction. Part 1. Bond Lengths in Organic Compounds. *Journal of the Chemical Society, Perkin Transactions 2* **1987**, 1-19.

15. Volkov, A.; Abramov, Y. A.; Coppens, P., Density-optimized radial exponents for X-ray charge-density refinement from *ab initio* crystal calculations. *Acta Crystallographica, Section A* **2001,** *57*, 272-282.

16. Clementi, E.; Raimondi, D. L., Atomic Screening Constants from SCF Functions. *J Chem Phys* **1963,** *38*, 2686-2689.

17. Coppens, P.; Gururow, T. N.; Leung, P.; Stevens, E. D.; Becker, P. J.; Yang, Y. W., Electron Population Analysis of Accurate Diffraction Data. VII. Net Atomic Charges and Molecular Dipole Moments from Spherical-Atom X-ray Refinements, and the Relation between Atomic Charge and Shape. *Acta Crystallographica, Section A* **1979,** *35*, 63-72.

18. Meindl, K.; Henn, J., Foundations of residual-density analysis. *Acta Crystallographica, Section A* **2008,** *64*, 404-418.

19. Bader, R. F. W., *Atoms in Molecules : A Quantum Theory*. Clarendon Press: Oxford, 1990; p xviii, 438 p.

20. Holladay, A.; Leung, P.; Coppens, P., Generalized Relations Between *d*-Orbital Occupancies of Transition-Metal Atoms and Electron-Density Multipole Population Parameters from X-ray-Diffraction Data. *Acta Crystallographica, Section A* **1983,** *39*, 377-387.

21. Viefhaus, T.; Schwarz, W.; Hubler, K.; Locke, K.; Weidlein, J., The variable reaction behaviour of base-free tris(trimethylsilyl)methyl lithium with trihalogenides of earth-metals and iron. *Z. Anorg. Allg. Chem.* **2001,** *627*, 715-725.

22. Genoni, A., X-ray Constrained Extremely Localized Molecular Orbitals: Theory and Critical Assessment of the New Technique. *J. Chem. Theory Comput.* **2013,** *9*, 3004-3019.

23. Obara, S.; Saika, A., Efficient recursive computation of molecular integrals over Cartesian Gaussian functions. *J. Chem. Phys.* **1986,** *84*, 3963-3974.

24. Head-Gordon, M.; Pople, J. A., A method for two-electron Gaussian integral and integral derivative evaluation using recurrence relations. *J. Chem. Phys.* **1988,** *89*, 5777-5786.

25. Volkov, A.; Macchi, P.; Farrugia, L. J.; Gatti, C.; Mallinson, P. R.; Richter, T.; Koritsanszky, T. *XD2015 - a computer program for multipole refinement, topological analysis of charge densities and evaluation of intermolecular energies from experimental or theoretical structure factors.* , v1.04; University at Buffalo, State University of New York, Buffalo, NY, University of Milano, Milano, Italy, University of Glasgow, Glasgow, U.K., CNRISTM, Milano, Italy, and Middle Tennessee State University Murfreesboro, TN, 2015.

26. Fischer, A.; Tiana, D.; Scherer, W.; Batke, K.; Eickerling, G.; Svendsen, H.; Bindzus, N.; Iversen, B. B., Experimental and Theoretical Charge Density Studies at Subatomic Resolution. *J. Phys. Chem. A* **2011,** *115*, 13061-13071.
27. Platts, J. A.; Overgaard, J.; Jones, C.; Iversen, B. B.; Stasch, A., First Experimental Characterization of a Non-nuclear Attractor in a Dimeric Magnesium(I) Compound. *J. Phys. Chem. A* **2011,** *115*, 194-200.
28. Overgaard, J.; Jones, C.; Stasch, A.; Iversen, B. B., Experimental Electron Density Study of the Mg-Mg Bonding Character in a Magnesium(I) Dimer. *J. Am. Chem. Soc.* **2009,** *131*, 4208-+.
29. Cruickshank, D. W. J.; Rollett, J. S., Electron-Density Errors at Special Positions. *Acta Crystallogr* **1953,** *6*, 705-707.
30. Rees, B., Variance and Covariance in Experimental Electron Density Studies, and Use of Chemical Equivalence. *Acta Crystallographica, Section A* **1976,** *32*, 483-488.
31. Quickplot. https://github.com/mrvj/QuickPlot (accessed November 1st, 2018).
32. Hirshfeld, F. L., Can X-Ray Data Distinguish Bonding Effects from Vibrational Smearing? *Acta Crystallographica, Section A* **1976,** *32*, 239-244.
33. Zhurov, V. V.; Zhurova, E. A.; Pinkerton, A. A., Optimization and evaluation of data quality for charge density studies. *J Appl Crystallogr* **2008,** *41*, 340-349.
34. Jørgensen, M. R. V., Personal Communication. Program may be obtained upon contacting the authors.
35. Abrahams, S. C.; Keve, E. T., Normal Probability Plot Analysis of Error in Measured and Derived Quantities and Standard Deviations. *Acta Crystallographica, Section A* **1971,** *A 27*, 157-165.
36. Stash, A. *DRK Plot Version 1.00.014*, Moscow, 2007.
37. Macrae, C. F.; Bruno, I. J.; Chisholm, J. A.; Edgington, P. R.; McCabe, P.; Pidcock, E.; Rodriguez-Monge, L.; Taylor, R.; van de Streek, J.; Wood, P. A., *Mercury CSD 2.0* - new features for the visualization and investigation of crystal structures. *J Appl Crystallogr* **2008,** *41*, 466-470.